

# Breaking Imitation Bottlenecks: Reinforced Diffusion Powers Diverse Trajectory Generation

Ziying Song, Lin Liu, Hongyu Pan, Bencheng Liao, Mingzhe Guo, Lei Yang,  
Yongchang Zhang, Shaoqing Xu, Caiyan Jia, Yadan Luo

**Abstract**—Existing end-to-end autonomous driving (E2E-AD) methods predominantly rely on single expert demonstrations through imitation learning, often leading to conservative and homogeneous driving behaviors that struggle to generalize to complex real-world scenarios. In this work, we propose **DIVER**, a novel E2E-AD framework that combines diffusion-based multi-mode trajectory generation with reinforcement learning to produce diverse, safe, and goal-directed trajectories. First, the model conditions on map elements and surrounding agents to generate multiple reference trajectories from each ground-truth reference trajectory that overcome the inherent limitations of single-mode imitation. Second, we treat the diffusion process as a stochastic policy and employ Group Relative Policy Optimization (GPRO) objectives to guide the diffusion process. By optimizing trajectory-level rewards for both diversity and safety, GPRO directly mitigates mode collapse and enhances collision avoidance, encouraging exploration beyond expert demonstrations and ensuring physically plausible plans. Furthermore, to address the limitations of L2-based open-loop metrics in capturing trajectory diversity, we propose a novel trajectory diversity metric to evaluate the diversity of multi-mode predictions. Extensive experiments on the closed-loop NAVSIM and Bench2Drive benchmarks, as well as the open-loop nuScenes dataset, demonstrate that DIVER significantly improves trajectory diversity, effectively addressing the mode collapse problem inherent in imitation learning.

**Index Terms**—Autonomous Driving, End-to-End Autonomous Driving, Diffusion Model, Reinforcement Learning.

## 1 INTRODUCTION

IN recent years, autonomous driving has entered a new phase, with significant progress in end-to-end autonomous driving (E2E-AD) [10, 11]. E2E-AD systems integrate traditionally independent tasks—such as 3D object detection, multi-object tracking, online mapping, motion prediction and planning—into a unified framework that directly learns driving policies from raw sensor inputs [1, 2, 3, 4, 5, 6]. Among these tasks, planning serves as a core module that not only directly governs ego-vehicle decision-making and control but also provides implicit guidance to upstream perception tasks [1].

Currently, imitation learning (IL) continues to serve as the predominant methodology for planning task in autonomous driving systems [10]. IL enables E2E-AD methods to mimic human expert driving behaviors through supervised learning, typically by minimizing the distance between predicted trajectories and ground truth (GT) trajectories. In the early stages, E2E-AD methods [1, 2, 5, 6] primarily adopted single-mode trajectory, as shown in Figure 1 (a), which predicts a single trajectory through regression. However, it struggles to handle complex traffic scenarios

- Ziying Song, Lin Liu, Mingzhe Guo and Caiyan Jia are with Beijing Key Laboratory of Traffic Data Mining and Embodied Intelligence, School of Computer Science and Technology, Beijing Jiaotong University. Email: 22110110@bjtu.edu.cn. Ziying Song contributed to this work as an intern at Horizon Robotics.
- Hongyu Pan, Bencheng Liao, and Yongchang Zhang are with Horizon Robotics.
- Lei Yang is with School of Mechanical and Aerospace Engineering, Nanyang Technological University, Singapore.
- Shaoqing Xu is with University of Macau, China
- Yadan Luo is with the School of Electrical Engineering and Computer Science, The University of Queensland, Australia.

Corresponding author: Caiyan Jia.

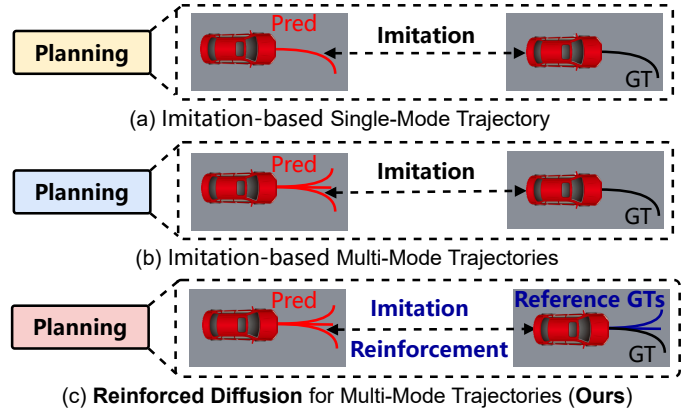


Fig. 1: (a) **Imitation-based Single-Mode Trajectory Planning** [1, 2, 3, 4, 5, 6, 7] predicts deterministic trajectories but lacks action diversity, leading to potential safety risks. (b) **Imitation-based Multi-Mode Trajectories Planning** [3, 4, 8, 9] fails to address the diversity loss in imitation learning end-to-end autonomous driving, leading to mode collapse. The generated multi-mode trajectories overly depend on a single GT trajectory, ultimately clustering around it. (c) **The proposed DIVER framework** adopts reinforced diffusion for multi-mode trajectory generation, encouraging the ego-vehicle to produce diverse driving behaviors instead of rigidly following a single expert.

due to neglecting the uncertainties of the driving environment and interactions with other traffic participants. To address the limitations of single-mode trajectory generation, subsequent studies [3, 4, 8, 9] have proposed multi-mode trajectories prediction frameworks, as illustrated in Figure 1

(b). For instance, VADv2 [8] employs probabilistic modeling techniques to capture potential driving intentions and generate multiple proposal trajectories, ultimately selecting the optimal trajectory through a maximum scoring mechanism. However, these approaches [3, 4, 8, 9] still suffer from mode collapse, where the generated multi-mode trajectories exhibit excessive dependence on GT trajectories. This results in multi-mode trajectories distributions that are overly concentrated around the GT, failing to adequately represent the true diversity of driving behaviors. Mode collapse is a form of diversity loss in multi-mode trajectories prediction [10]. Its root cause is the strong reliance of IL methods on a single expert trajectory. Regardless of open-loop or closed-loop training, and whether in single-mode or multi-mode prediction, most IL methods are trained using a single GT expert trajectory as the target, limiting the learning of diverse driving behaviors.

Some autonomous driving methods [12, 13] leverage diffusion models to generate diverse trajectories. Diffusion models [14], as a powerful generative learning framework, have demonstrated strong capabilities in modeling multi-mode behavior distributions for robotic policy learning [15]. Introducing diffusion models into E2E-AD trajectory planning has emerged as a promising research direction. For instance, DiffusionDrive [4] combines truncated diffusion strategies with efficient cascaded diffusion decoders to mitigate the loss of trajectory diversity during IL training. However, since its optimization process still adheres to the IL framework based on a single expert trajectory, the generated multi-mode trajectories ultimately tend to converge toward a single GT. This limitation prevents the model from fully overcoming the inherent constraints of imitation learning.

Although diffusion models [16] demonstrate strong capabilities in multi-mode trajectories generation, their training still primarily relies on maximum likelihood estimation. While conditional constraints can provide some guidance, the lack of explicit supervision for safety often leads to physically infeasible trajectories in real-world scenarios. Recent works such as DeepSeek-R1 [17] have leveraged reinforcement learning (RL) to enhance reasoning capabilities, while AlphaDrive [18] and RAD [19] have validated the effectiveness of RL in E2E-AD. Unlike conventional supervised learning, RL directly evaluates and optimizes generation results based on designed reward functions without requiring explicit labels. Motivated by this, we propose to integrate reinforcement learning with diffusion models by designing diversity and safety rewards as external optimization signals. This approach effectively overcomes the limitations of traditional supervision (e.g., L2 loss) and guides the diffusion model to generate safe, physically plausible, and diverse future trajectories.

In this work, we propose **DIVER**, a novel multi-mode E2E-AD framework that leverages reinforcement learning to guide diffusion models for generating diverse, feasible trajectories (Figure 1(c)). By leveraging diffusion models, our approach generates multiple plausible future trajectories, capturing a spectrum of driving behaviors while maintaining safety and feasibility. Specifically, we introduce the Policy-Aware Diffusion Generator (PADG), which incorporates map elements and surrounding agents as conditions and generates diverse multi-mode trajectories and multiple

reference GTs, guided by a single GT trajectory and trajectory anchors, effectively capturing various driving styles. To ensure both safety and diversity in trajectory planning, we incorporate reinforcement learning to supervise the diffusion process via reward signals, enabling optimization of generated trajectories under diversity and safety constraints. Additionally, to address the misalignment between conventional open-loop metrics (primarily L1Loss) and the intrinsic requirement for diverse trajectory generation, we introduce a novel **Diversity Metric** to better evaluate the diversity of multi-mode trajectories predictions. Extensive experiments on closed-loop **Bench2Drive** and **NAVSIM**, as well as open-loop **nuScenes**, demonstrate that our DIVER significantly enhances trajectory diversity and planning robustness, effectively addressing the mode collapse issue in imitation learning.

Overall, our contributions are as follows:

- We propose the **DIVER**, an novel multi-mode E2E-AD framework that uses reinforcement learning to guide diffusion models in generating diverse and feasible driving behaviors.
- We introduce the **Policy-Aware Diffusion Generator (PADG)**, which incorporates map elements and agent interactions as conditional inputs, enabling the generation of multi-mode trajectories that capture diverse driving styles.
- We leverage reinforcement learning to guide the diffusion model with diversity and safety rewards, addressing the limitations of imitation learning.
- We propose a novel **Diversity Metric** to evaluate multi-mode trajectories generation, providing a more principled way to assess the diversity and effectiveness of generated trajectories compared to existing metrics.
- Extensive evaluations on the Bench2Drive, NAVSIM, NuScenes demonstrate that DIVER significantly improves the diversity, safety, and feasibility of generated trajectories over state-of-the-art methods.

## 2 RELATED WORK

### 2.1 End-to-end Autonomous Driving

End-to-end autonomous driving is a fully differentiable machine learning system that takes raw sensor input data and other metadata as prior information, directly outputting control signals or trajectory planning for vehicles [10, 11]. Early works [20, 21] excluded intermediate tasks, such as perception and motion prediction, which were characterized by limited interpretability and difficulties in optimization. UniAD[1], as a pioneering work, integrates perception tasks and planning tasks via Transformer[22], explicitly supervising 3D object detection [23, 24, 25], multi-object tracking[26], online mapping[27], motion prediction[28], occupancy prediction[29], and planning [30] tasks within a unified model. Subsequently, VAD[2] further explores the application of vectorized scene representation from MapTR [27] to enhance the efficiency of E2E-AD. DualAD [31] disentangles dynamic agents and static elements, compensating for motion effects and flexibly propagating the belief state over time. A series of E2E-AD works [1, 2, 5, 20, 31, 32],

represented by UniAD[1] and VAD[2], have adopted single-mode trajectory for planning performance. However, single-mode trajectory planning methods have issues with action diversity and associated safety risks. To address the above limitations, VADv2 [8] has recently shifted to a multi-mode planning framework by scoring and sampling from an extensive fixed vocabulary of anchor trajectories. Based on the design of multi-mode planning, SparseDrive [3] proposes a hierarchical planning selection strategy to select a rational and safe trajectory as the final planning output. HydraMDP [9] proposes a universal framework of end-to-end multi-mode planning via multi-target hydra-distillation. By leveraging historical trajectory momentum, MomAD [33] addresses the issue of inconsistent multi-mode trajectories over time. DiffusionDrive [4] leverages diffusion models to capture multi-mode action distributions in an E2E-AD framework. Existing multi-mode trajectories planning methods [3, 4, 8, 9, 33] do not fundamentally resolve mode collapse in imitation learning.

## 2.2 Diffusion Models for Autonomous Driving

Diffusion models approximate data distributions through iterative denoising and have demonstrated remarkable performance in image generation tasks [16], showing great potential for behavior modeling and trajectory generation in autonomous driving[34]. DiffScene[35] utilizes diffusion models to synthesize safe scenarios for evaluating autonomous driving safety. DiffBEV [36] adopts conditional diffusion to produce fine-grained BEV representations. MotionDiffuser [37] employs diffusion-based representations for multi-agent trajectory prediction. DiffusionDrive [4] models multi-mode trajectories distributions via a truncated diffusion process. VDT-Auto [38] integrates diffusion Transformers with vision-language models (VLMs) for action generation. MomAD[33] incorporates noise injection and denoising within the perception module to enhance robustness and generalization. DiffAD [39] formulates E2E-AD as a conditional image generation task by unifying heterogeneous driving objectives into a rasterized representation under a diffusion framework. DiFSD [40] introduces both position-level motion diffusion and trajectory-level planning denoising to model uncertainty, thereby enhancing the stability and convergence of the entire training framework. Overall, diffusion-based research in E2E-AD remains limited but holds great potential.

## 2.3 Reinforcement Learning for Autonomous Driving

Reinforcement Learning enables an agent to learn an optimal policy through interactions with the environment by maximizing cumulative long-term rewards [41]. Landmark achievements such as AlphaGo [42] and AlphaGo Zero [43] have demonstrated RL's remarkable capabilities in complex strategy games, while AlphaFold [44] has showcased its power in protein structure prediction. More recently, the successful application of RL in LLMs like DeepSeek-R1 [17] further validates its broad applicability and value. In autonomous driving, several works have begun to explore the integration of RL. Chen et al. [45] propose the 'world on rails' assumption, which simplifies RL by decoupling the

agent from the environment. GUMP [46] introduces an on-line training module to improve policy learning efficiency. Lu et al. [47] show that combining imitation learning with simple RL rewards significantly enhances the safety and reliability of learned driving policies. Toromanoff et al. [48] introduce implicit affordances to enable RL to handle urban driving scenarios, including lane keeping, pedestrian and vehicle avoidance, and traffic light interpretation. Zhang et al. [49] train an RL expert to map bird's-eye view images to low-level continuous actions, providing informative supervision for imitation learning agents. RAD [19] trains an end-to-end driving agent in a photorealistic 3DGS environment using RL. AlphaDrive [18] is among the first to integrate GRPO-based RL with planning and reasoning, substantially improving both performance and training efficiency in E2E-AD.

## 3 PRELIMINARY

### 3.1 End-to-End Autonomous Driving

Current E2E-AD systems are predominantly based on IL, which aims to learn expert driving policies by mapping raw sensor inputs to ego-vehicle trajectory outputs. It consists of several sequential or unified tasks, including 3D object detection, multi-object tracking, online mapping, motion prediction, and planning. 3D object detection and multi-object tracking tasks provide dynamic semantic features of surrounding agents for planning, while the online mapping module extracts high-confidence lane and road elements as static map features to assist trajectory planning. Among these, planning plays a central role, as it determines the final decision of the ego vehicle.

**Multi-Mode Trajectories.** The planning module typically predicts a sequence of future waypoints, represented as  $\tau = \{(x_t, y_t)\}_{t=1}^{T_f}$ , where  $(x_t, y_t)$  denotes the ego-vehicle position in its local coordinate frame at time step  $t$ , and  $T_f$  is the planning horizon. For datasets such as Bench2Drive[50] and nuScenes [51], trajectories are usually sampled at 2 Hz over a 3-second horizon, resulting in 6 waypoints. To enhance robustness, safety, and adaptability, E2E-AD systems increasingly incorporate diverse driving strategies. A common scheme to enable such diversity is through multi-mode trajectories prediction, where the system predicts  $M$  future trajectories, typically  $M = 6$ , denoted as  $\tau = \{(x_t^{(m)}, y_t^{(m)}) \mid t = 1, \dots, T_f; m = 1, \dots, M\}$ . The final trajectory is selected from these candidates based on scoring functions, and the diversity among them (e.g., turning, overtaking, following) is used to infer the ego-vehicle's potential driving strategies.

### 3.2 Diffusion Models for Driving Policy Diversity

Diffusion models, owing to their probabilistic generative nature and progressive denoising mechanism, offer unique advantages in modeling diverse driving strategies. Through iterative denoising, they can generate a wide distribution of high-quality candidate trajectories (e.g., lane changes, deceleration, or detours). However, most existing diffusion-based planning methods are still trained under the imitation learning (IL) paradigm, relying on a single expert trajectory

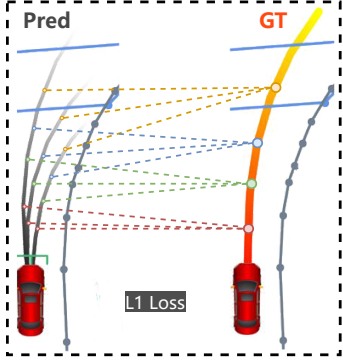


Fig. 2: **Imitation learning-based multi-mode trajectories paradigm.** Most IL-based multi-mode E2E-AD methods rely on L1 loss for training and L2 distance for evaluation, which emphasizes matching a single GT trajectory rather than modeling diversity. This misalignment limits the generation of truly diverse behaviors. Even with diffusion-based frameworks [4], such imitation-driven objectives constrain their capacity to capture multi-mode driving patterns.

as supervision, as shown in Figure 2. Under this setup, despite the strong generative capacity of diffusion models, the output multi-mode trajectories tend to collapse around the GT, exhibiting limited diversity. This raises a fundamental question: **Why do diffusion models struggle to generate diverse trajectories under imitation learning supervision?**

Under conventional imitation learning (IL) settings, where training is supervised by a single ground-truth (GT) trajectory, their ability to generate diverse behaviors is fundamentally constrained. We present a theoretical analysis to explain this limitation.

Let a trajectory be defined as a sequence of waypoints  $\tau = (x_t, y_t) t = 1^{T_f}$ , and a multi-mode output as  $\tau^{(m)} m = 1^M$ . In IL-based trajectory prediction, the training objective typically maximizes the log-likelihood of the observed trajectory:

$$\max_{\theta} \mathbb{E}_{\tau \sim p_{\text{data}}} [\log p_{\theta}(\tau)] \quad (1)$$

When the dataset provides only a single GT trajectory  $\tau^*$  per input, the data distribution reduces to a Dirac delta:

$$p_{\text{data}}(\tau) = \delta(\tau - \tau^*) \quad (2)$$

Consequently, the training objective simplifies to maximizing the likelihood of this unique trajectory:

$$\max_{\theta} \log p_{\theta}(\tau^*) \quad (3)$$

This forces the model to concentrate all probability mass on  $\tau^*$ , yielding a degenerate solution:

$$p_{\theta}^{\text{opt}}(\tau) = \delta(\tau - \tau^*) \quad (4)$$

Diffusion models are trained by minimizing a denoising score-matching loss, often expressed as:

$$\min_{\theta} \mathbb{E}_{\epsilon \sim \mathcal{N}(0, I)} \left[ \|\epsilon - \epsilon_{\theta}(\tau^* + \sqrt{\alpha_t} \epsilon, t)\|^2 \right] \quad (5)$$

This formulation teaches the model to reconstruct  $\tau^*$  from noisy perturbations, effectively collapsing all modes

toward the single GT trajectory. No matter how strong the underlying generative process is, the diversity of output trajectories  $\tau^{(m)} m = 1^M$  collapses around  $\tau^*$ , failing to reflect genuine multi-modeity.

We further analyze the diversity loss via the covariance of the output distribution:

$$\Sigma = \mathbb{E}_{\tau \sim p_{\theta}} [(\tau - \mu)(\tau^* - \mu)^T], \quad \mu = \mathbb{E}[\tau] \quad (6)$$

With all  $\tau$  approximating  $\tau^*$ , we have  $\mu \approx \tau^*$  and  $\Sigma \approx 0$ , indicating near-zero diversity across predicted trajectories.

In summary, diffusion-based E2E-AD methods trained under single-GT supervision inherit the same mode collapse issue as standard IL, despite their generative capacity. To address this, we propose a hybrid IL-RL training framework, DIVER, that introduces diversity-aware rewards to encourage multi-mode, safe trajectories generation.

## 4 DIVER

### 4.1 Overall Architecture

As shown in Figure 3, we propose **DIVER**, a novel E2E-AD framework that integrates diffusion models and reinforcement learning to enable diverse, and safe multi-mode trajectories. **DIVER** consists of two main components: perception module and motion planner, which takes raw perception features as input and outputs a distribution over future trajectories. At the training paradigm level, **DIVER** adopts a hybrid learning scheme that combines IL with RL. The core innovations of **DIVER** lie in two aspects. First, the **Policy-Aware Diffusion Generator (PADG)** generates diverse trajectory candidates by leveraging a diffusion model conditioned not only on a single expert trajectory but also on multiple Reference GTs, capturing a range of plausible human-like driving behaviors such as lane changes, yielding, and overtaking. Second, we leverage reinforcement learning to guide the diffusion-based trajectory generation process, addressing the inherent limitations of IL-based supervision and aligning the output with safety and diversity objectives. Overall, **DIVER** combines the generative capability of diffusion models with the optimization strength of reinforcement learning, forming a flexible and scalable framework for E2E-AD. It enables the system to explore a broader solution space in complex scenarios while ensuring the physical feasibility and behavioral safety of the generated trajectories.

### 4.2 Policy-Aware Diffusion Generator.

To overcome the limitations of conservative and mode-collapsed behaviors in IL-based E2E-AD, we propose the Policy-Aware Diffusion Generator (PADG). PADG is a core component of our DIVER that enables diverse, and feasible trajectory generation through a conditional denoising diffusion process. Specifically, PADG is built upon a conditional diffusion framework, which reconstructs multi-mode future trajectory distributions from random noise through iterative denoising, guided at each step by rich scene semantics as conditional information. It consists of a dual-branch architecture: one branch learns to reconstruct the distribution of the predicted trajectory, while the other models the expert trajectory to serve as guidance.

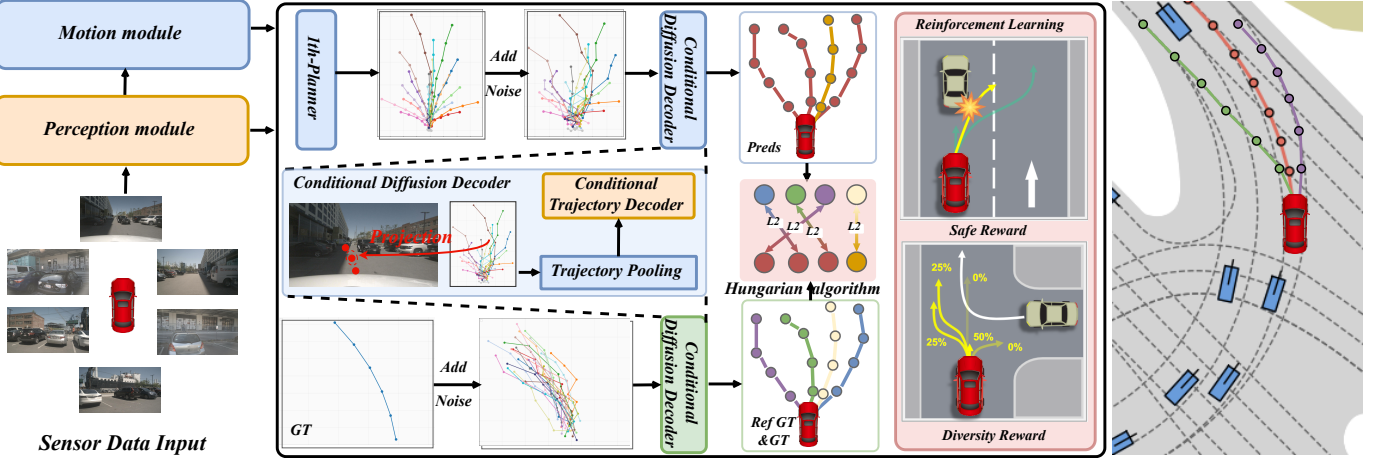


Fig. 3: **The overall architecture of DIVER.** As a multi-mode trajectories E2E-AD framework, DIVER first encodes multi-view images into feature maps to extract scene representations through a perception module. It then predicts the motion of surrounding agents and performs planning via a conditional diffusion model guided by reinforcement learning to generate diverse multi-intention trajectories. Our approach effectively addresses the inherent mode collapse in imitation learning, enabling the generation of safe and diverse behaviors for complex driving scenarios.

#### 4.2.1 Diverse Multi-Mode Trajectories Forward Diffusion.

To generate diverse and informative future trajectory distributions, we apply a forward diffusion process to multiple trajectory types, including multi-mode predicted trajectories, anchor proposals, and the GT trajectory. This step aims to perturb the trajectories with Gaussian noise in a controlled manner, enabling the conditional diffusion model to learn a robust denoising process that captures the underlying multi-modality of future motion.

Specifically, let  $\tau_0^{(m)} \in \mathbb{R}^{T \times 2}$  denote a predicted future trajectory of mode  $m$ ,  $\tau_0^{a(m)}$  denote its associated anchor proposal, and  $\tau_0^{gt}$  the GT future trajectory. At each diffusion step  $t = 1, \dots, T$ , the trajectories are corrupted with Gaussian noise following the standard forward diffusion process:

$$q(\tau_t^{(m)} | \tau_0^{(m)}) = \mathcal{N}(\tau_t^{(m)}; \sqrt{\alpha_t} \tau_0^{(m)}, (1 - \alpha_t) \mathbf{I}), \quad (7)$$

$$q(\tau_t^{a(m)} | \tau_0^{a(m)}) = \mathcal{N}(\tau_t^{a(m)}; \sqrt{\alpha_t} \tau_0^{a(m)}, (1 - \alpha_t) \mathbf{I}), \quad (8)$$

$$q(\tau_t^{gt} | \tau_0^{gt}) = \mathcal{N}(\tau_t^{gt}; \sqrt{\alpha_t} \tau_0^{gt}, (1 - \alpha_t) \mathbf{I}) \quad (9)$$

where  $\alpha_t \in (0, 1)$  is the noise schedule at timestep  $t$ . This formulation ensures that the model can learn to recover high-quality trajectory samples from various noise levels during training, while preserving the structured correlations between predicted and anchor trajectories.

By jointly applying noise to both predicted and anchor trajectories, we encourage the model to explore the latent trajectory space more broadly, leading to greater trajectory diversity during generation. Simultaneously, injecting noise into the GT trajectory supports supervised learning of the denoising objective, grounding the generative process in realistic motion patterns.

#### 4.2.2 Conditional Diffusion Decoder.

To effectively guide the denoising process in the conditional diffusion model, we incorporate rich scene semantics, in-

cluding the BEV map, agent, and anchor trajectory features, into the trajectory generation process.

Given noisy multi-mode trajectories  $\tilde{\tau}_t^{(m)}$  and their corresponding anchor trajectories  $\tau_t^{a(m)}$ , we extract spatio-temporal features through sinusoidal position embedding and transformer-based encoding. Specifically, we first apply a forward diffusion process to perturb the trajectories with Gaussian noise. Let  $\tilde{\tau}^{(m)}$  denote the noised multi-mode trajectories after de-normalization. We then construct high-dimensional embeddings as:

$$\mathcal{E}^{(m)} \tau = \text{PE}(\tilde{\tau}^{(m)}), \mathcal{F}^{(m)} \tau = \text{Enc}(\mathcal{E}^{(m)} \tau), \quad (10)$$

$$\mathcal{E}^{(m)} \tau^a = \text{PE}(\tilde{\tau}^{a(m)}), \mathcal{F}^{(m)} \tau^a = \text{Enc}(\mathcal{E}^{(m)} \tau^a), \quad (11)$$

where  $\text{PE}(\cdot)$  denotes sine-based positional encoding, and  $\text{Enc}(\cdot)$  is a lightweight transformer encoder that captures the temporal dynamics and structural properties of the noisy trajectories. These embeddings are used for subsequent conditional interaction with the scene features.

To guide the generation of diverse and feasible future trajectories, we design a conditional diffusion decoder that performs multi-mode interaction between the noisy trajectory features and high-level semantic cues from the driving scene. This module also incorporates a GT-based reference trajectory to inject goal-oriented inductive bias.

Given the GT trajectory  $\tau^{GT}$  and its diffusion noise  $\epsilon \sim \mathcal{N}(0, I)$ , we obtain noisy trajectories using the forward process of the diffusion scheduler:

$$\tilde{\tau}_t^{(m)} = q_t(\tau^{GT}, \epsilon) = \sqrt{\bar{\alpha}_t} \tau^{GT} + \sqrt{1 - \bar{\alpha}_t} \epsilon, \quad (12)$$

where  $t$  denotes the diffusion step and  $\bar{\alpha}_t$  the cumulative noise factor. We first embed both the noisy predicted trajectory  $\tilde{\tau}_t^{(m)}$  and the corresponding reference trajectory

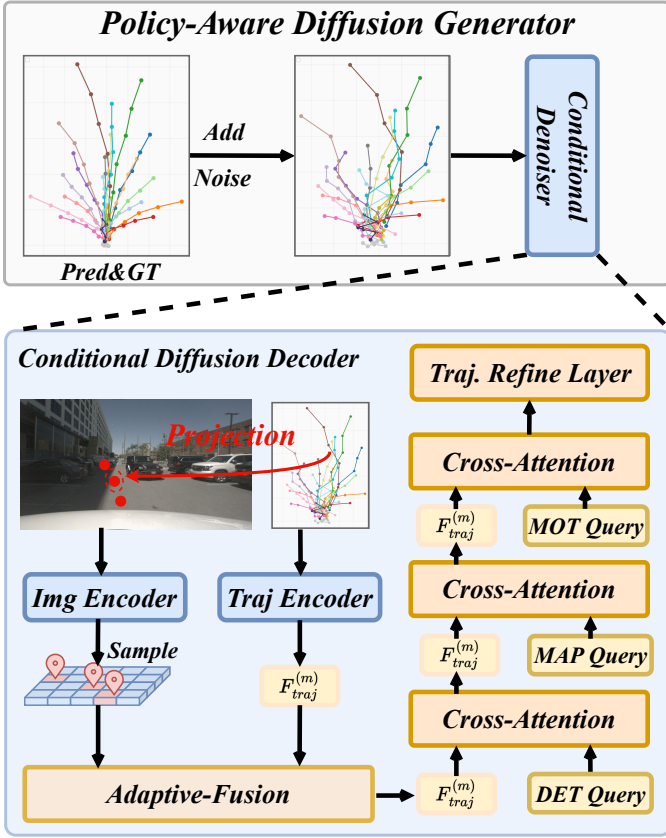


Fig. 4: The illustration of Policy-Aware Diffusion Generator. By incorporating the predicted trajectory, GT trajectory, and anchor trajectory as inputs, PADG reconstructs diverse multi-mode trajectories from noise through a conditional denoising process, guided by map and agent context.

$\tau^{\text{ref}(m)}$  to extract their spatial-temporal semantic features. The embedding process is defined as:

$$\mathcal{F}_\tau^{(m)} = \text{PE} \left( \phi \left( \tilde{\tau} t^{(m)} \right) \right), \quad (13)$$

$$\mathcal{F}_{\text{ref}}^{(m)} = \text{PE} \left( \phi \left( \tau^{\text{ref}(m)} \right) \right), \quad (14)$$

where  $\phi(\cdot)$  denotes the sine-cosine positional embedding applied to each trajectory waypoint, i.e.,  $\phi(\cdot) = \text{SineEmbed}(\cdot)$ ,  $\text{PE}(\cdot)$  denotes the trajectory position encoder, typically implemented as a lightweight MLP or transformer block,  $\mathcal{F}_\tau^{(m)}$  and  $\mathcal{F}_{\text{ref}}^{(m)}$  are the learned representations of the noisy predicted trajectory and the reference trajectory for mode  $m$ , respectively.

To effectively model the interaction between noisy trajectory predictions and multi-mode contextual information, we design a two-stage conditional feature fusion pipeline, as detailed in Algorithm 1 and 2.

In the first stage, we apply a trajectory-aware image feature pooling module, referred to as TrajPooler (Algorithm 1). Given a noisy trajectory  $\hat{\tau}^{(m)}$ , we first recover its absolute coordinates via cumulative sum. We then sparsely sample 3D points along the trajectory and project them onto the image plane using the known camera intrinsics  $\mathbf{K}$  and extrinsics  $\mathbf{T}$ . These projected 2D locations are used to extract multi-scale image features from the BEV encoder's output. To adaptively aggregate these image features, we learn

### Algorithm 1: Trajectory pooling

---

**Input:** Noisy trajectory  $\hat{\tau}^{(m)} \in \mathbb{R}^{T \times 2}$ , Trajectory feature  $F_{\text{traj}}^{(m)} \in \mathbb{R}^d$ , Multi-scale image features  $\mathcal{F}_{\text{img}}$ , Camera intrinsics  $\mathbf{K}$ , Extrinsics  $\mathbf{T}$   
**Output:** Trajectory-aware fused feature  $F_{\text{traj}}^{(m)}$

- 1 **Convert to absolute positions:**  
 $\tau^{(m)} \leftarrow \text{CumulativeSum}(\hat{\tau}^{(m)})$
- 2 **Generate 3D keypoints along trajectory:**  
 $P^{(m)} \leftarrow \text{Sample3DPoints}(\tau^{(m)})$
- 3 **Project to image planes:**  
 $u^{(m)} \leftarrow \text{ProjectTo2D}(P^{(m)}, \mathbf{K}, \mathbf{T})$
- 4 **Sample multi-scale image features:**  
 $F_{2D}^{(m)} \leftarrow \text{SampleImageFeatures}(\mathcal{F}_{\text{img}}, u^{(m)})$
- 5 **Learned attention weights:**  
 $\alpha^{(m)} \leftarrow \text{AttentionWeights}(F_{\text{traj}}^{(m)}, \mathbf{K}, \mathbf{T})$
- 6 **Fused trajectory feature:**  
 $F_{\text{traj}}^{(m)} \leftarrow \text{MLP}(\sum \alpha^{(m)} \cdot F_{2D}^{(m)}) + F_{\text{traj}}^{(m)}$

---

attention weights  $\alpha^{(m)}$  conditioned on the initial trajectory feature  $F_{\text{traj}}^{(m)}$ . The fused trajectory feature  $F_{\text{traj}}^{(m)}$  is obtained via a weighted sum followed by an MLP and residual fusion with the original instance embedding.

In the second stage, we inject the pooled trajectory token into a transformer-based conditional decoder, as shown in Algorithm 2. Specifically, we follow a hierarchical attention stack where the trajectory token  $F_{\text{traj}}^{(m)}$  is first used to query agent-level memory via multi-head cross-attention (MHCA), producing agent-conditioned features  $F_{\text{agent}}^{(m)}$ . These are further refined by attending to map-level memory features, yielding  $F_{\text{map}}^{(m)}$ . Finally, navigation-level anchors (e.g., waypoints from reference plans or diffusion priors) are fused via another MHCA block. The final output  $F_{\text{out}}^{(m)}$  is obtained by feeding the resulting feature through a residual FFN block.

Together, this conditional feature interaction pipeline ensures that the predicted trajectory at each diffusion step is semantically grounded in both visual context and structural priors, enhancing both diversity and plausibility of multi-mode predictions.

#### 4.2.3 Reference GTs-Guided Multi-Mode Trajectories.

**Planning Head.** After the final conditional decoding step, the predicted multi-mode trajectories  $\hat{\tau}^{(m)}$  are reconstructed from the final trajectory token  $F_{\text{out}}^{(m)}$  via a lightweight MLP-based regression head. These predicted trajectories are not generated independently: each is explicitly guided by a GT-based reference trajectory  $\tau^{\text{ref}(m)}$ , which provides a mode-aligned semantic anchor for generation.

Specifically, during training, each predicted trajectory mode is paired with a GT-derived reference trajectory that encodes distinct motion intents (e.g., turning, yielding, or lane-changing). By injecting the reference into the conditional decoder and using it to shape the context-aware feature fusion, our model learns to align each mode with a feasible, interpretable, and scene-compliant motion pattern.

**Algorithm 2:** Conditional Trajectory Decoder

---

**Input:**

Trajectory token  $F_{\text{traj}}^{(m)} \in \mathbb{R}^d$ ,  
Agent memory tokens  $\mathcal{F}_{\text{agent}} \in \mathbb{R}^{N_a \times d}$  with  $\mathbf{P}_{\text{agent}}$ ,  
Map memory tokens  $\mathcal{F}_{\text{map}} \in \mathbb{R}^{N_m \times d}$  with  $\mathbf{P}_{\text{map}}$ ,  
Navigation memory  $\mathcal{F}_{\text{nav}}^{(m)} \in \mathbb{R}^{T \times d}$ ,  
Planning query  $Q^{(m)}$

**Output:** Multi-Mode Trajectories:  $F_{\text{out}}^{(m)}$

- 1 **Agent-Level Cross Attention:**  $F_{\text{agent}}^{(m)} = \text{MHCA}(Q^{(m)} + F_{\text{traj}}^{(m)}, \mathcal{F}_{\text{agent}} + \mathbf{P}_{\text{agent}}, \mathcal{F}_{\text{agent}})$
- 2 **Map-Level Cross Attention:**  $F_{\text{map}}^{(m)} = \text{MHCA}(Q^{(m)} + F_{\text{agent}}^{(m)}, \mathcal{F}_{\text{map}} + \mathbf{P}_{\text{map}}, \mathcal{F}_{\text{map}})$
- 3 **Anchor-Level Cross Attention:**  $F_{\text{nav}}^{(m)} = \text{MHCA}(F_{\text{map}}^{(m)}, \mathcal{F}_{\text{nav}}^{(m)}, \mathcal{F}_{\text{nav}}^{(m)})$
- 4 **Final LayerNorm + FFN:**  $F_{\text{out}}^{(m)} = \text{FFN}(\text{LayerNorm}(F_{\text{nav}}^{(m)}) + F_{\text{nav}}^{(m)})$

---

At inference time, the model samples multiple noise vectors  $\epsilon^{(m)} \sim \mathcal{N}(0, I)$  and generates corresponding multi-mode trajectories  $\hat{\tau}^{(m)}$  via the denoising diffusion process. The reference trajectories  $\tau^{\text{ref}(m)}$  can be drawn from anchor plans, plan queries, or diffusion priors, ensuring that the output space spans diverse yet goal-directed behaviors.

**Matching Loss for Diverse Trajectories.** To promote the generation of diverse and plausible trajectories, we introduce a matching loss between predicted multi-mode trajectories and reference GT trajectories. Instead of supervising the model to regress toward a single GT trajectory, we sample reference GT trajectories from the empirical distribution of expert behaviors and match them to the model's predicted multi-mode trajectories. Specifically:

We denote the predicted trajectory set as  $\hat{\tau}^{(1)}, \dots, \hat{\tau}^{(M)}$  and the reference GTs set as  $\tau^{\text{ref}(1)}, \dots, \tau^{\text{ref}(M)}$ . We apply the **Hungarian algorithm** to compute an optimal one-to-one matching between predicted and reference trajectories by minimizing the pairwise  $\ell_2$  distance:

$$\mathcal{L}_{\text{match}} = \frac{1}{M} \sum_{m=1}^M \left\| \hat{\tau}^{(m)} - \tau^{\text{ref}(m)} \right\|_2^2 \quad (15)$$

This strategy enforces that each predicted mode is assigned to a distinct reference, which directly encourages the diffusion model to explore multiple plausible futures rather than collapsing to a mean or dominant mode.

This reference-guided design not only enhances trajectory diversity by explicitly modeling distinct semantic intents, but also ensures goal feasibility and safety by grounding each mode in plausible motion priors. This is particularly crucial for addressing the mode collapse and over-conservative behaviors that plague prior IL-based E2E-AD methods.

### 4.3 Reinforcement Learning for Trajectory Planning

#### 4.3.1 Overview of Group Relative Policy Optimization

Group Relative Policy Optimization (GRPO) is a reinforcement learning algorithm tailored for multi-agent or multi-mode scenarios, where agent policies are updated relative to

a shared group baseline. Unlike standard PPO [52], GRPO [53] formulates the policy gradient as a relative advantage over group-conditioned expectations, thereby encouraging diverse yet cooperative behaviors. The GRPO objective is given by:

$$\mathcal{J}_{\text{GRPO}}(\theta) = \mathbb{E}_{q, \{o_i\} \sim \pi_{\theta_{\text{old}}}} \left[ \frac{1}{G} \sum_{i=1}^G \mathcal{L}_i - \beta \mathbb{D}_{KL}(\pi_{\theta} \| \pi_{\text{ref}}) \right], \quad (16)$$

$$\mathcal{L}_i = \min(w_i A_i, \text{clip}(w_i, 1 - \epsilon, 1 + \epsilon) A_i), \quad (17)$$

where,  $w_i = \frac{\pi_{\theta}(o_i | q)}{\pi_{\theta_{\text{old}}}(o_i | q)}$ ,  $\epsilon$  and  $\beta$  are hyper-parameters, and the advantage  $A_i$  is computed using the normalized reward within the group.

#### 4.3.2 GRPO for Trajectory Planning

Despite their strong capability in multi-mode trajectories generation, diffusion models still face two critical limitations in end-to-end autonomous driving (E2E-AD): (i) mode collapse, where generated trajectories converge to similar patterns, and (ii) lack of safety awareness, leading to kinematically feasible yet unsafe motions. These issues largely stem from reliance on single-GT supervision and the absence of explicit guidance for task-specific objectives such as behavioral diversity and safety.

To address this, we treat the diffusion model as a stochastic policy and introduce a reinforcement learning objective based on Group Relative Policy Optimization (GRPO) [53], which augments the standard imitation learning pipeline with trajectory-level rewards. GRPO enables direct optimization over non-differentiable objectives, facilitates exploration beyond expert demonstrations, and improves policy robustness by aligning generation with safety and diversity constraints. This hybrid optimization paradigm steers the diffusion process toward producing diverse, safe, and goal-directed trajectories that better support the downstream planning requirements of E2E-AD.

We define a composite reward function  $r(\hat{\tau})$  that evaluates each trajectory in terms of *diversity* and *safety*. The detailed formulations of the Diversity Reward  $r_{\text{div}}$  and Safety Reward  $r_{\text{safe}}$  are presented below.

**Diversity Reward  $r_{\text{div}}$ .** To encourage multi-mode trajectories generation and mitigate mode collapse, we design a diversity reward  $r_{\text{div}}$  that quantifies the pairwise dissimilarity among predicted trajectories. Given a set of  $M$  predicted trajectories  $\{\hat{\tau}^{(1)}, \hat{\tau}^{(2)}, \dots, \hat{\tau}^{(M)}\}$ , we compute:

$$r_{\text{div}} = \frac{2}{M(M-1)} \sum_{i=1}^M \sum_{j=i+1}^M \left\| \hat{\tau}^{(i)} - \hat{\tau}^{(j)} \right\|_2 \quad (18)$$

This reward promotes diverse trajectory generation by maximizing inter-trajectory distances, encouraging the diffusion model to explore a broader set of plausible behaviors rather than collapsing to redundant modes. It is differentiable and seamlessly integrates with GRPO to guide the policy toward both diversity and feasibility.

**Safety Reward  $r_{\text{safe}}$ .** To ensure the feasibility and risk-awareness of generated trajectories, we introduce a safety reward that penalizes predicted paths with low clearance from static or dynamic obstacles. We define a differentiable

distance-based cost function using a safety map  $D_{\text{safe}}(\mathbf{x})$ , which encodes inverse proximity to obstacles. For a trajectory  $\hat{\tau} = \hat{x} * t * t = 1^T$ , the safety reward is computed as:

$$r_{\text{safe}}(\hat{\tau}) = -\frac{1}{T} \sum_{t=1}^T \mathbb{I}[D_{\text{safe}}(\hat{x} * t) < d * \text{thresh}], \quad (19)$$

where  $\mathbb{I}[\cdot]$  is an indicator function and  $d_{\text{thresh}}$  is a safety margin. This term penalizes any predicted point too close to obstacles, promoting collision-free behaviors. Integrated with the GRPO objective, this safety-aware reward guides the diffusion model to sample physically plausible and safe trajectories in complex, dynamic environments.

**Planing Loss for Diverse Trajectories.** The total reward for a predicted trajectory  $\hat{\tau}^{(m)}$  is defined as:

$$r(\hat{\tau}^{(m)}) = r_{\text{div}}(\hat{\tau}^{(m)}) + \lambda_{\text{safe}} \cdot r_{\text{safe}}(\hat{\tau}^{(m)}). \quad (20)$$

The reward is integrated into a reinforcement learning loss under the GRPO framework:

$$\mathcal{L}_{\text{RL}} = -\mathbb{E}_{\hat{\tau}^{(m)} \sim \pi_{\theta}} [\text{GRPO}(\hat{\tau}^{(m)}, r(\hat{\tau}^{(m)}))] \quad (21)$$

This formulation enables the diffusion model to adaptively steer its sampling process toward trajectories that are diverse, feasible, and physically plausible.

The complete training objective combines imitation learning and reinforcement learning:

$$\mathcal{L}_{\text{total}} = \lambda_{\text{match}} \mathcal{L}_{\text{match}} + \lambda_{\text{RL}} \mathcal{L}_{\text{RL}} \quad (22)$$

Here,  $\lambda_{\text{match}}$  and  $\lambda_{\text{RL}}$  are weighting coefficients balancing the contributions of trajectory matching and policy optimization.

Our reinforcement-augmented training framework addresses key limitations of diffusion-based planners in E2E-AD. Through reward-guided GRPO optimization, we impose safety and diversity constraints that are not captured by conventional MSE-based training. This hybrid supervision strategy bridges the gap between behavior cloning and policy-level optimization, leading to a more robust and deployable planning solution.

## 5 EXPERIMENTS

### 5.1 Dataset

**Bench2Drive (Close-Loop).** We conduct training and evaluation of DIVER on the **Bench2Drive** [50], a closed-loop evaluation protocol based on the CARLA Leaderboard 2.0 [54] for E2E-AD. It provides a base training set of 1000 clips, with 950 used for training and 50 for open-loop validation. Each clip captures approximately 150 meters of continuous driving in a specific traffic scenario. For closed-loop evaluation, we use the official 220 routes, covering 44 interactive scenarios with 5 routes each.

**NAVSIM (Close-Loop).** We conduct training and evaluation of DIVER on the **NAVSIM** [55] dataset. NAVSIM is a real-world, planning-oriented dataset that builds upon OpenScene [56], a compact redistribution of nuPlan [57], the largest publicly available annotated driving dataset. It leverages eight cameras to achieve a full 360° field of view, along with a merged LiDAR point cloud derived from five sensors. Annotations are provided at 2 Hz and include

both HD maps and object bounding boxes. The dataset is specifically designed to emphasize challenging driving scenarios involving dynamic changes in driving intentions, while deliberately excluding trivial cases such as stationary scenes or constant-speed cruising.

**NuScenes (Open-Loop).** We conduct extensive open-loop experiments on the **nuScenes** dataset [51], which consists of 1000 driving scenes (700 for training, 150 for validation and 150 for test). Each scene lasts 20 seconds and includes around 40 key-frames annotated at 2 Hz. Each sample contains six images from surround-view cameras (covering 360° FOV), and point clouds from both LiDAR and radar sensors.

**Turning-nuScenes (Open-Loop).** We conduct extensive open-loop experiments on the **Turning-nuScenes** dataset [58], a challenging subset of NuScenes proposed by MomAD [58] to evaluate trajectory consistency in non-trivial maneuvers. While most planning tasks in the original nuScenes dataset primarily involve go-straight commands, Turning-nuScenes specifically focuses on turning scenarios to assess the temporal coherence of predicted trajectories. To construct this subset, samples are selected based on a displacement threshold of 25 meters between the predicted positions at 0.5s and 3.0s in the GT ego trajectory. The resulting validation set comprises 680 samples across 17 scenes, accounting for approximately one-tenth of the full nuScenes validation set.

**Adv-nuSc (Open-Loop).** To evaluate adversarial robustness, we conduct extensive open-loop experiments on the **Adv-nuSc** [59] dataset. It contains 156 scenes (6,115 samples) and is specifically crafted to challenge the ego vehicle by introducing adversarial traffic participants. It is built upon the validation split of the nuScenes dataset [51], which contains 150 scenes, each with 20 seconds of driving data. For each scene, we randomly select up to 10 background vehicles (if there are that many) that come close to the ego vehicle at any point in time and designate them as candidate adversarial agents. Challenger is then used to generate adversarial trajectories for these vehicles, creating diverse and challenging driving scenarios.

**NuScenes-C (Open-Loop).** **NuScenes-C** [60] is a corrupted benchmark derived from the nuScenes validation set, introducing various types of noise to assess the robustness of planning models. It includes 27 corruption types applied at 5 severity levels. To evaluate robustness under adverse weather conditions, we select three representative weather corruptions — Rain, Snow, and Fog — as our test scenarios.

### 5.2 Evaluation Metrics

**Close-Loop (Bench2Drive).** The **Bench2Drive** [50] includes five metrics for closed-loop evaluation: Driving Score (DS), Success Rate (SR), Efficiency, Comfortness, and Multi-Ability. The Success Rate quantifies the proportion of routes successfully completed within the allotted time. The Driving Score follows CARLA [11], incorporating both route completion status and violation penalties, where infractions reduce the score via discount factors. Efficiency and Comfortness are used to measure the speed performance and comfort of the autonomous driving system during the driving process, respectively. Multi-Ability measures 5 advanced skills, including 'Merging', 'Overtaking', 'Emergency

Brake, Give Way, and Traffic Sign', independently for urban driving.

**Close-Loop (NAVSIM).** NAVSIM benchmarks planning performance using nonreactive simulations and closed-loop metrics for comprehensive evaluation. In this paper, we employ the proposed PDM score (PDMS) [55], which is a weighted combination of several sub-scores: no at-fault collisions (NC), drivable area compliance (DAC), time-to-collision (TTC), comfort (Comf.), and ego progress (EP).

**Open-Loop.** For the **nuScenes** dataset [51], **Adv-nuSc** [59], **Turning-nuScenes** [58], and **nuScenes-C** [60], we adopt the commonly used **collision rate** to assess planning performance, as in SparseDrive [3].

We argue that the **L2 distance** is *not* a suitable evaluation metric for multi-mode E2E-AD methods, as it only measures proximity to a single GT trajectory and fails to capture the benefits of multi-mode prediction. To address this, we introduce a new **Diversity Metric** (denoted as **Div**) to better evaluate the variety and richness of predicted trajectories. This metric is designed to be scale-invariant, modality-invariant, and bounded within  $[0, 1]$ , making it suitable for consistent comparison across models and scenarios.

Let  $M$  be the number of predicted modes (e.g.,  $M = 6$ ), and  $T$  the number of waypoints per trajectory (e.g.,  $T = 6$ ). Each trajectory consists of 2D coordinates, with  $\mathbf{p}_t^{(i)} = (x_t^{(i)}, y_t^{(i)})$  denoting the  $t$ -th waypoint of the  $i$ -th trajectory.

To characterize the temporal variation in trajectory diversity, we compute a time-conditioned diversity score at each future timestamp. For example, in the Bench2Drive and nuScenes datasets, we consider  $t \in \{0.5, 1.0, 1.5, 2.0, 2.5, 3.0\}$  seconds. We first compute the unnormalized pairwise diversity as:

$$D_{\text{raw}}^{(t)} = \frac{2}{M(M-1)} \sum_{i=1}^{M-1} \sum_{j=i+1}^M \left\| \mathbf{p}_t^{(i)} - \mathbf{p}_t^{(j)} \right\|_2. \quad (23)$$

To ensure comparability across scenes with varying trajectory scales, we normalize it using the mean trajectory magnitude:

$$\text{Div.}^{(t)} = \min \left( 1, \frac{D_{\text{raw}}^{(t)}}{\epsilon + \frac{1}{M} \sum_{m=1}^M \left\| \mathbf{p}_t^{(m)} \right\|_2} \right), \quad (24)$$

where  $\epsilon$  is a small constant (e.g.,  $10^{-6}$ ) to avoid division by zero.

Overall, a higher **Diversity** value indicates greater dispersion among the predicted trajectories, reflecting a richer coverage of intent modes such as lane changes, braking, and yielding. When Diversity approaches 1, the predicted modes are highly diverse and well-separated in the trajectory space. Conversely, a value near 0 suggests that the predicted trajectories are highly similar, indicating a lack of behavioral diversity. Notably, the Diversity Metric is only applicable to multi-mode trajectories E2E-AD methods.

### 5.3 Implementation Details

To demonstrate the generalization capability of **DIVER**, we conduct experiments against several strong E2E-AD

baselines, including **SparseDrive** [3], **VAD** [2], and **TransFuser** [5]. On the **Bench2Drive** [50], **nuScenes** [51], and **Adv-nuSc** [59] datasets, we compare against **SparseDrive** and **VAD**. For nuScenes and Adv-nuSc, we adopt ResNet-50 [68] as the image backbone with an input resolution of  $256 \times 704$ . The detection module operates within a circular range of 55 meters, and the online mapping covers a  $60 \times 30$  meter area (longitudinal  $\times$  lateral). The motion module generates 6 trajectory candidates (modes). On **Bench2Drive**, we use ResNet-50 with 6 decoder layers and an input resolution of  $640 \times 352$ . We also define fixed numbers of hybrid task queries: 900 agent queries, 100 map queries, and 480 planning queries. On the **NAVSIM** [55] dataset, we adopt **TransFuser** [5] as the baseline and follow the standard Navtrain split for training. For fair comparison, we use the same perception modules and ResNet-34 backbone as in TransFuser. All experiments are conducted on a server with 8 NVIDIA RTX 4090 (24GB) GPUs.

## 5.4 Main Results

To comprehensively evaluate the multi-mode trajectories generation capability of our proposed **DIVER**, we conduct **closed-loop** experiments on two representative E2E-AD benchmarks: **Bench2Drive** and **NAVSIM**, as shown in Tables 1 and 2. In Table 3, we further present **open-loop** results on the **NuScenes** dataset. Additionally, Table 1 includes supplementary **open-loop** evaluation results on **Bench2Drive**. It is important to note that we do *not* adopt the conventional **L2 distance** in open-loop evaluation. This is because L2 distance merely reflects the proximity between a predicted trajectory and a single GT trajectory, failing to capture the diversity and spread of multi-mode trajectories predictions. Relying solely on this metric compromises the core objective of multi-mode trajectory generation—namely, to cover a wide range of plausible future intents.

### 5.4.1 Close-Loop Results

**Bench2Drive (Close-Loop).** We report closed-loop results on the Bench2Drive dataset, which features 44 diverse interactive scenarios. DIVER significantly outperforms VAD, VAD<sub>mmt</sub>, MomAD, and SparseDrive across all planning metrics. Compared to VAD<sub>mmt</sub>, it improves Success Rate by 11.8%, Comfortness by 8.6%, Driving Score by 4.1%, and Efficiency by 4.0%. Against SparseDrive, DIVER achieves even larger gains: +29.0% in Success Rate, +12.5% in Comfortness, +10.5% in Driving Score, and +4.0% in Efficiency. These results highlight DIVER's ability to produce more successful, comfortable, and stable trajectories in complex scenarios. Moreover, in multi-ability evaluation, DIVER achieves the highest average score, with notable gains in overtaking (+3.78%) and emergency braking (+5.51%), reflecting improved decision-making and semantic awareness. This demonstrates that DIVER not only improves planning robustness but also enables flexible driving behaviors.

**NAVSIM (Close-Loop).** As shown in Table 2, our proposed DIVER achieves the better overall performance across all closed-loop metrics on the NAVSIM planning-oriented benchmark. This benchmark evaluates planners under non-reactive simulations using multiple dimensions, including No at-fault Collisions (NC), Drivable Area Compliance (DAC), Time-to-Collision (TTC), Comfort (Comf.),

TABLE 1: **Open-Loop**, **Closed-Loop** results and Multi-Ability results on Bench2Drive (V0.0.3) under base training set. ‘mmt’ refers multi-mode trajectories variant of VAD and  $\dagger$  denotes the re-implementation. \* denotes expert feature distillation. ‘DS’ denotes Driving Score. ‘SR’ denotes Success Rate. ‘Effi’ denotes Efficiency. ‘Comf’ denotes Comfortness. ‘Merg.’ denotes Merging. ‘Overta.’ denotes Overtaking. ‘Emerge.’ denotes Emergency Brake. It is worth noting that the *Diversity Metric* ( $Div^{(t)} \uparrow$ ) is applicable only to multi-mode E2E-AD methods.

Method	Traj. Scheme	Venue	Open-loop Metric		Closed-loop Metric						Multi-Ability(%) $\uparrow$					
			Avg.	L2 $\downarrow$	Avg.	$Div^{(t)} \uparrow$	DS $\uparrow$	SR (%) $\uparrow$	Effi $\uparrow$	Comf $\uparrow$	Merg. $\uparrow$	Overta. $\uparrow$	Emerge. $\uparrow$	Give Way $\uparrow$	Traffic Sign $\uparrow$	Mean
TCP-traj* <sup>[20]</sup>	ST	IL	NeurIPS 2022	1.70	-	59.90	30.00	76.54	18.08	8.89	24.29	51.67	40.00	46.28	34.22	
ThinkTwice* <sup>[61]</sup>	ST	IL	CVPR 2023	0.95	-	62.44	31.23	69.33	16.22	27.38	18.42	35.82	50.00	54.23	37.17	
DriveAdapter* <sup>[62]</sup>	ST	IL	ICCV 2023	1.01	-	64.22	33.08	70.22	16.01	28.82	26.38	48.76	50.00	56.43	42.08	
Raw2Drive*	ST	RL	Arxiv 2025	-	-	71.36	50.24	214.17	22.42	43.35	51.11	60.00	50.00	62.26	53.34	
DriveTrans* <sup>[63]</sup>	MT	IL	ICLR 2025	0.62	-	63.46	35.01	100.64	20.78	17.57	35.00	48.36	40.00	52.10	38.60	
WoTE* <sup>[64]</sup>	ST	IL	Arxiv 2025	-	-	61.71	31.36	-	-	-	-	-	-	-	-	
DiffAD* <sup>[39]</sup>	MT	IL	Arxiv 2025	1.55	-	67.92	38.64	-	-	-	-	-	-	-	-	
ThinkTwice <sub>mmt</sub> * <sup>†</sup> <sup>[61]</sup>	MT	IL	CVPR 2023	0.93	0.19	63.34	33.23	71.56	18.32	31.31	21.23	38.33	50.00	57.45	37.17	
DIVER (Ours)	MT	IL&RL	-	1.11	0.38	68.90	36.75	72.34	22.34	35.08	25.09	41.09	50.00	59.21	42.09	
AD-MLP <sup>[65]</sup>	ST	IL	Arxiv 2023	3.64	-	18.05	0.00	48.45	22.63	0.00	0.00	0.00	0.00	4.35	0.87	
UniAD-Base <sup>[1]</sup>	ST	IL	CVPR 2023	0.73	-	45.81	16.36	129.21	43.58	14.10	17.78	21.67	10.00	14.21	15.55	
VAD <sup>[2]</sup>	ST	IL	ICCV 2023	0.91	-	42.35	15.00	157.94	46.01	8.11	24.44	18.64	20.00	19.15	18.07	
GenAD <sup>[66]</sup>	ST	IL	ECCV 2024	-	-	44.81	15.90	-	-	-	-	-	-	-	-	
MomAD(VAD) <sup>[58]</sup>	MT	IL	CVPR 2025	0.87	0.18	45.35	17.44	162.09	49.34	9.99	26.31	20.07	20.00	20.23	19.32	
MomAD(SD) <sup>[58]</sup>	MT	IL	CVPR 2025	0.82	0.20	47.91	18.11	174.91	51.20	13.21	21.02	18.01	20.00	21.07	18.66	
VAD <sub>mmt</sub> <sup>†</sup> <sup>[2]</sup>	MT	IL	ICCV 2023	0.89	0.20	42.87	15.91	158.12	47.22	9.43	25.31	19.91	20.00	20.09	18.95	
DIVER (Ours)	MT	IL&RL	-	1.13	0.32	47.95	19.47	164.66	51.28	13.83	29.09	25.51	20.00	24.93	22.67	
SparseDrive <sup>†</sup> <sup>[3]</sup>	MT	IL	ICRA 2025	0.87	0.21	44.54	16.71	170.21	48.63	12.18	23.19	17.91	20.00	20.98	17.45	
DIVER (Ours)	MT	IL&RL	-	1.05	0.35	49.21	21.56	177.00	54.72	15.98	28.22	23.71	20.00	24.38	22.46	

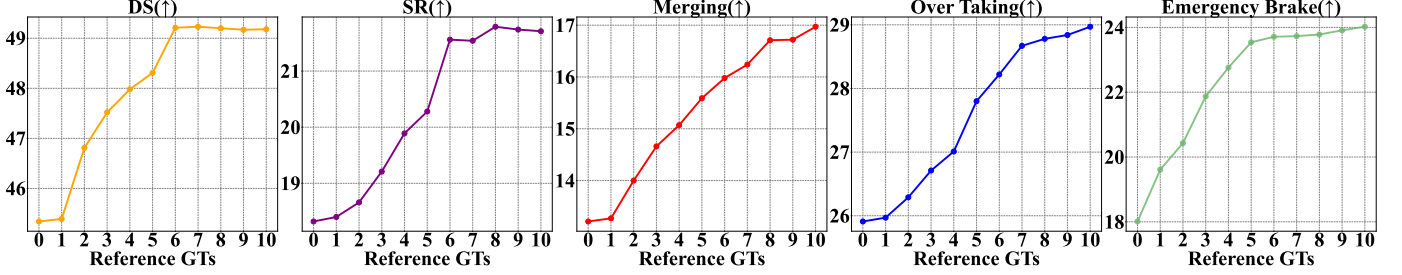


Fig. 5: Impact of the Number of Reference GTs on Closed-Loop Performance (Bench2Drive). A value of 0 indicates no reference GTs (only the GT trajectory is used). Values of 1 and above correspond to using one reference GTs in addition to the GT, and so on.

TABLE 2: Comparison on planning-oriented NAVSIM navtest split with **Closed-Loop** metrics. ‘mmt’ refers multi-mode trajectories variant of TransFuser and \* denotes the re-implementation.

Method	Input	NC $\uparrow$	DAC $\uparrow$	TTC $\uparrow$	Comf. $\uparrow$	EP $\uparrow$	PDMS $\uparrow$
UniAD [1]	C	97.8	91.9	92.9	100	78.8	83.4
LTF [5]	C	97.4	92.8	92.4	100	79.0	83.8
PARA-Drive [67]	C	97.9	92.4	93.0	99.8	79.3	84.0
VADv2 [8]	C&L	97.2	89.1	91.6	100	76.0	80.9
Hydra-MDP [9]	C&L	98.3	96.0	94.6	100	78.7	86.5
DiffusionDrive [4]	C&L	98.2	96.2	94.7	100	82.2	88.1
TransFuser [5]	C&L	97.7	92.8	92.8	100	79.2	84.0
TransFuser <sub>mmt</sub> * [5]	C&L	96.2	95.4	90.7	100	80.7	85.1
DIVER (Ours)	C&L	<b>98.5</b>	<b>96.5</b>	<b>94.9</b>	100	<b>82.6</b>	<b>88.3</b>

Ego Progress (EP), and the Planning-Driven Metric Score (PDMS) [55]. DIVER attains the highest PDMS score of **88.3**, outperforming strong baselines such as TransFuser<sub>mmt</sub> and DiffusionDrive, which achieve 87.5 and 86.1, respectively. In terms of safety, DIVER leads with the highest NC score of **98.5**, indicating fewer at-fault collisions. Moreover, DIVER demonstrates excellent planning feasibility and smoothness with top scores in DAC (**96.5**) and Comf. (**100**), while maintaining strong forward progress (EP: **82.6**). These results

TABLE 3: Planning results on the **Open-Loop** NuScenes [51] validation dataset. It is worth noting that the *Diversity Metric* ( $Div^{(t)} \uparrow$ ) is applicable only to multi-mode E2E-AD methods like MomAD [58], DiffusionDrive [4], and SparseDrive [3].

Method	$Div^{(t)} \uparrow$				Col. Rate (%) $\downarrow$			
	1s	2s	3s	Avg.	1s	2s	3s	Avg.
UniAD [1]	-	-	-	-	0.62	0.58	0.63	0.61
VAD [2]	-	-	-	-	0.03	0.19	0.43	0.21
MomAD [58]	0.05	0.10	0.19	0.11	<b>0.01</b>	<b>0.05</b>	0.22	0.09
DiffusionDrive [4]	0.07	0.14	0.24	0.15	0.03	<b>0.05</b>	0.16	0.08
SparseDrive [3]	0.05	0.11	0.23	0.13	<b>0.01</b>	<b>0.05</b>	0.18	0.08
DIVER (Ours)	<b>0.10</b>	<b>0.19</b>	<b>0.34</b>	<b>0.21</b>	<b>0.01</b>	<b>0.05</b>	<b>0.15</b>	<b>0.07</b>

highlight DIVER’s ability to balance safety, comfort, and goal-directed planning, demonstrating its effectiveness in realistic driving simulations. The improvements across all aspects suggest that our method not only generates diverse multi-mode trajectories but also ensures their practical executability and robustness in closed-loop scenarios.

TABLE 4: Robustness study of planning results on the Turning-nuScenes [58] validation dataset. \* denotes the re-implementation.

Method	Div. <sup>(t)</sup> ↑				Col. Rate (%) ↓			
	1s	2s	3s	Avg.	1s	2s	3s	Avg.
SparseDrive [3]	0.09	0.18	0.36	0.21	0.04	0.17	0.98	0.40
DiffusionDrive* [4]	0.11	0.21	0.37	0.23	<b>0.03</b>	0.14	0.85	0.34
MomAD [58]	0.09	0.17	0.34	0.20	<b>0.03</b>	0.13	0.79	0.32
DIVER (Ours)	<b>0.17</b>	<b>0.29</b>	<b>0.47</b>	<b>0.31</b>	<b>0.03</b>	<b>0.11</b>	<b>0.67</b>	<b>0.27</b>

TABLE 5: Robustness study of planning performance on Adv-nuSc under adversarial driving scenarios.

Method	Col. Rate (%) ↓			
	1s	2s	3s	Avg.
UniAD [1]	0.800%	4.100%	6.960%	3.950%
VAD [2]	4.460%	7.590%	9.080%	7.050%
SparseDrive [3]	<b>0.029%</b>	0.618%	2.430%	1.026%
DiffusionDrive [4]	0.068%	1.299%	3.646%	1.671%
DIVER (Ours)	0.033%	<b>0.423%</b>	<b>1.798%</b>	<b>0.752%</b>

#### 5.4.2 Open-Loop Results

**NuScenes (Open-Loop).** As shown in Table 3, DIVER demonstrates superior performance on the nuScenes dataset in both diversity and safety. For multi-mode trajectory generation, it achieves Diversity Metric scores of 0.10, 0.19, 0.34 at 1s, 2s, and 3s, with an average of 0.21—representing a 61.5% improvement over DiffusionDrive (avg. 0.15). This indicates more intention-aware and temporally balanced trajectory generation. In terms of safety, DIVER reduces the average collision rate to 0.07, compared to 0.08 from DiffusionDrive, achieving a 12.5% reduction. Notably, this improvement in diversity does not come at the cost of safety. These results confirm the effectiveness of DIVER in producing diverse and safe trajectories.

**Bench2Drive (Open-Loop).** As shown in Table 1, DIVER achieves significantly higher diversity in Open-Loop evaluation on the Bench2Drive dataset. It reaches a score of 0.32 compared to 0.20 for VAD<sub>mmt</sub> and 0.18 for MomAD, marking a 60.0% improvement. Against SparseDrive (0.21), DIVER scores 0.35, improving by 66.7%. These results highlight DIVER’s stronger ability to generate diverse and intention-rich trajectories.

### 5.5 Robustness Study

To validate the robustness of DIVER under diverse and challenging conditions, we conduct comprehensive evaluations on turning-heavy scenarios (Turning-nuScenes [58], Table 4), adversarial perturbation settings (Adv-nuSc [59], Table 5), and adverse weather conditions (nuScenes-C [60], Table 6). Additionally, as shown in Table 7, we analyze long-horizon trajectory prediction performance on the nuScenes dataset.

#### 5.5.1 Adversarial Driving Challenging

**Turning-Heavy Scenarios (Turning-nuScenes).** As shown in Table 4, the Turning-nuScenes validation set evaluates planning robustness under complex turning conditions. DIVER exhibits superior trajectory diversity and safety. It achieves Diversity Metric scores of 0.17, 0.29, and 0.47 at 1s, 2s, and 3s, respectively (avg. 0.31), significantly surpassing DiffusionDrive (avg. 0.20) and MomAD (avg. 0.19). This

TABLE 6: Robustness study of planning performance on nuScenes-C.

Scene	Method	Col. Rate (%) ↓			
		1s	2s	3s	Avg.
Clean	SparseDrive [3]	<b>0.01</b>	<b>0.05</b>	0.18	0.08
	MomAD [58]	<b>0.01</b>	<b>0.05</b>	0.22	0.09
	DiffusionDrive [4]	0.03	<b>0.05</b>	0.16	0.08
	DIVER (Ours)	<b>0.01</b>	<b>0.05</b>	<b>0.15</b>	<b>0.07</b>
Snow	SparseDrive [3]	0.13	0.27	0.50	0.30
	MomAD [58]	0.08	0.16	0.30	0.18
	DiffusionDrive [4]	0.09	0.24	0.39	0.24
	DIVER (Ours)	<b>0.07</b>	<b>0.13</b>	<b>0.25</b>	<b>0.15</b>
Rain	SparseDrive [3]	0.11	0.27	0.55	0.31
	MomAD [58]	0.06	0.17	0.31	0.18
	DiffusionDrive [4]	0.07	0.18	0.35	0.20
	DIVER (Ours)	<b>0.05</b>	<b>0.16</b>	<b>0.27</b>	<b>0.16</b>
Fog	SparseDrive [3]	0.14	0.36	0.58	0.36
	MomAD [58]	0.06	0.19	0.32	0.19
	DiffusionDrive [4]	0.06	0.18	0.30	0.18
	DIVER (Ours)	<b>0.04</b>	<b>0.16</b>	<b>0.25</b>	<b>0.15</b>

TABLE 7: Long-horizon planning results on the nuScenes validation sets. We train models for 10 epochs for 6s-horizon prediction. \* denotes the re-implementation.

Method	Div. <sup>(t)</sup> ↑			Col. Rate (%) ↓		
	4s	5s	6s	4s	5s	6s
SparseDrive [3]	0.35	0.46	0.59	0.87	1.54	2.33
DiffusionDrive* [4]	0.36	0.47	0.62	0.84	1.46	2.19
MomAD [58]	0.33	0.43	0.52	0.83	1.43	2.13
DIVER (Ours)	<b>0.50</b>	<b>0.61</b>	<b>0.75</b>	<b>0.76</b>	<b>1.32</b>	<b>1.91</b>

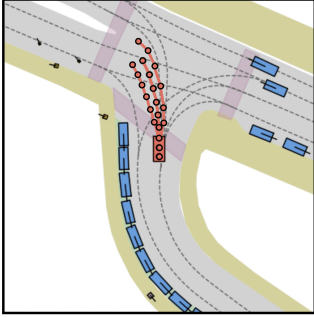
demonstrates DIVER’s ability to generate rich and diverse trajectory modes. In terms of safety, DIVER yields the lowest Collision Rate across all horizons (avg. 0.11), marking a 50.0% reduction compared to MomAD (avg. 0.22), indicating its robustness in multi-turn driving scenarios.

**Adversarial Perturbation Settings (Adv-nuSc).** Table 5 reports results on the Adv-nuSc benchmark, which introduces adversarial perturbations to challenge planning robustness. DIVER achieves the lowest Collision Rate across all horizons: 0.033%, 0.423%, and 1.798% at 1s, 2s, and 3s, respectively, with an average of 0.752%. This significantly outperforms prior methods such as UniAD (3.95%), VAD (7.05%), SparseDrive (2.06%), and DiffusionDrive (1.67%). These results highlight DIVER’s strong resilience under adversarial disturbances and its potential for deployment in safety-critical autonomous driving systems.

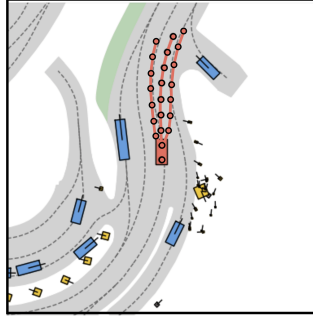
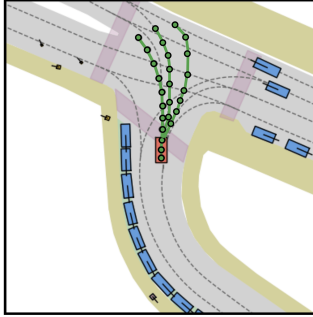
**Robustness in Noisy-Weather Scenarios (nuScenes-C).** As shown in Table 6, DIVER consistently achieves the lowest collision rates across all weather conditions, including clean, snow, rain, and fog. In the clean condition, DIVER records an average collision rate of only 0.05%, comparable to the best-performing baseline (MomAD: 0.05%). Under challenging conditions like snow, rain, and fog, DIVER exhibits greater robustness, with average collision rates of 0.09%, 0.15%, and 0.21%, respectively. These results represent a notable reduction compared to baselines such as SparseDrive (0.17% in snow, 0.35% in rain, 0.32% in fog) and DiffusionDrive (0.13%, 0.18%, and 0.26%). This highlights DIVER’s strong generalization and safety performance under various weather disturbances, demonstrating its practical viability in real-world scenarios.

TABLE 8: Ablation Study on Policy-Aware Diffusion Generator on Bench2Drive. ‘Condition’ denotes map and agent conditioning in the diffusion model, while ‘Reference GTs’ refers to reference trajectory guidance.

Method	Open-loop Metric		Closed-loop Metric				Multi-Ability(%) ↑				
	Avg. $Div_{(t)} \uparrow$	DS ↑	SR (%) ↑	Effi ↑	Comf ↑	Merg.	Overtra.	Emerge.	Give Way	Traffic Sign	Mean
SparseDrive	0.21	44.54	16.71	170.21	48.63	12.18	23.19	17.91	20.00	20.98	17.45
+ Condition	0.24	45.34	18.32	173.00	50.34	13.21	25.91	18.01	20.00	22.87	20.00
+ Reference GTs	0.29	47.12	19.89	172.86	51.31	14.02	26.38	18.78	20.00	22.91	20.42
DIVER	0.35	49.21	21.56	177.00	54.72	15.98	28.22	23.71	20.00	24.38	22.46



(a) DiffusionDrive(Left) VS DriveStyle(Right)



(b) DiffusionDrive(Left) VS DriveStyle(Right)

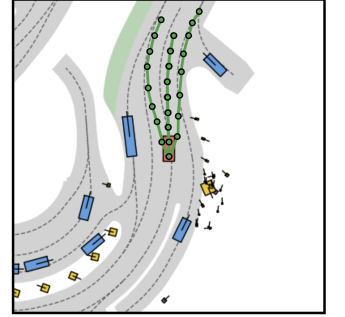


Fig. 6: Visualization results of DIVER compared with DiffusionDrive [4] on the NAVSIM [55] dataset. Our proposed DIVER generates significantly more diverse and feasible trajectories across various driving scenarios.

TABLE 9: Ablation Study on Policy-Aware Diffusion Generator on NAVSIM dataset. ‘Condition’ denotes map and agent conditioning in the diffusion model, while ‘Reference GTs’ refers to reference trajectory guidance.

Method	NC↑	DAC ↑	TTC↑	Comf.↑	EP↑	PDMS↑
TransFuser <sub>mmt</sub> *	96.2	95.4	90.7	100	80.7	85.1
+ Condition	96.2	96.3	90.8	100	81.2	86.3
+ Reference GTs	97.6	95.7	91.5	100	81.6	86.4
DIVER	98.5	96.5	94.9	100	82.6	88.3

TABLE 10: Ablation Study on Policy-Aware Diffusion Generator on NuScenes dataset. ‘Condition’ denotes map and agent conditioning in the diffusion model, while ‘Reference GTs’ refers to reference trajectory guidance.

Method	$Div_{(t)} \uparrow$			
	1s	2s	3s	Avg.
SparseDrive	0.05	0.11	0.23	0.13
+ Condition	0.06	0.15	0.26	0.16
+ Reference GTs	0.08	0.18	0.29	0.18
DIVER	0.10	0.19	0.34	0.21

### 5.5.2 Long-Horizon Planning

In Table 7, we evaluate long-horizon planning ability on nuScenes with a 6-second prediction horizon. DIVER achieves the highest Diversity Metric across all prediction timestamps, with 0.50, 0.61, and 0.75 at 4s, 5s, and 6s respectively (avg. 0.62), clearly outperforming all baselines. Compared to SparseDrive (avg. 0.43) and DiffusionDrive (avg. 0.49), this corresponds to a 44.2% and 26.5% relative improvement. Additionally, DIVER reports the lowest average collision rate (1.91%), significantly better than

TABLE 11: Ablation Study on Loss Function Design on NuScenes dataset.

Loss	$Div_{(t)} \uparrow$			
	1s	2s	3s	Avg.
L1 Loss	0.06	0.12	0.23	0.14
L1 Loss+ $\mathcal{L}_{RL}(PPO)$	0.06	0.14	0.25	0.15
$\mathcal{L}_{match}$	0.06	0.14	0.24	0.15
$\mathcal{L}_{match}+\mathcal{L}_{RL}(PPO)$	0.09	0.19	0.32	0.20
$\mathcal{L}_{match}+\mathcal{L}_{RL}(GRPO)$	0.10	0.19	0.34	0.21

TABLE 12: Ablation Study on Loss Function Design on NAVSIM dataset.

Method	NC↑	DAC ↑	TTC↑	Comf.↑	EP↑	PDMS↑
L1 Loss	96.5	95.5	90.9	100	81.0	85.5
L1 Loss+ $\mathcal{L}_{RL}(PPO)$	96.9	95.5	91.0	100	81.2	85.9
$\mathcal{L}_{match}$	97.6	93.2	92.1	100	82.1	86.7
$\mathcal{L}_{match}+\mathcal{L}_{RL}(PPO)$	98.1	95.4	94.1	100	82.3	87.9
$\mathcal{L}_{match}+\mathcal{L}_{RL}(GRPO)$	98.5	96.5	94.9	100	82.6	88.3

DiffusionDrive (2.19%) and MomAD (2.33%). These results confirm that DIVER not only ensures multi-mode diversity over extended horizons but also maintains high safety performance, which is crucial for stable long-term planning in autonomous driving systems.

## 5.6 Ablation Study

### 5.6.1 Ablation Study on PADG

**Effect of Condition and Reference GTs.** As shown in Tables 8, 9, and 10, our ablation studies on Bench2Drive[50], NAVSIM[55], and NuScenes[51] validate the effectiveness of the PADG in enhancing both diversity and safety in trajectory generation. Condition refers to the incorporation of map and agent information into the diffusion process,

enabling more context-aware and structurally grounded predictions. This leads to improved multi-modeity (14.3% increase in  $Div^{(t)}$  on Bench2Drive) and enhanced planning safety and comfort (NC +0.1%, PDMS +1.2 on NAVSIM). Reference GTs, on the other hand, introduce multiple high-quality trajectory anchors to guide the diffusion process beyond a single expert demonstration. This mitigates mode collapse and encourages diverse yet feasible trajectory generation. The integration of Reference GTs further boosts closed-loop performance (DS +1.78, SR +1.57% on Bench2Drive) and improves navigation robustness (TTC +0.8 on NAVSIM). When both components are combined in DIVER, we observe consistent state-of-the-art results across all benchmarks. These results demonstrate that context conditioning and reference guidance play complementary roles in generating diverse, safe, and realistic driving behaviors. **Impact of the Number of Reference GTs.** As shown in Figure 5, increasing the number of Reference GTs leads to consistent gains in Driving Score, Success Rate, and complex maneuvers (e.g., merging, overtaking). Performance stabilizes around 6–7 GTs, indicating that moderate reference diversity effectively enhances planning robustness and behavioral richness.

### 5.6.2 Ablation Study on Loss Function Design

As shown in Tables 11 and 12, loss function design has a significant impact on model performance. On the NuScenes dataset, the standard L1 loss fails to exploit the potential of diffusion and reference GTs, yielding limited diversity (Avg.  $Div.\uparrow = 0.14$ ). Even when combined with RL (PPO), improvements are marginal. In contrast, replacing L1 with the proposed matching loss  $\mathcal{L}_{\text{match}}$  enables the model to benefit from trajectory diversity, yielding higher  $Div^{(t)}$  (up to 0.21). Further integrating RL with diversity and safety rewards enhances performance, especially using GRPO, which outperforms PPO in both diversity and planning quality. On NAVSIM,  $\mathcal{L}_{\text{match}} + \mathcal{L}_{\text{RL(GRPO)}}$  achieves the best PDMS (88.3), confirming that this design effectively balances realism, diversity, and safety.

### 5.7 Visualization

As shown in Figure 6, we present a qualitative comparison between DiffusionDrive and our proposed DIVER in representative turning scenarios. DIVER produces a broader spread of trajectories that better capture diverse driving intentions. This highlights its ability to overcome the limitations of imitation learning, which often leads to conservative and mode-collapsed behaviors.

## 6 CONCLUSION

The proposed DIVER framework addresses a key challenge in end-to-end autonomous driving: the planning model collapse commonly observed in imitation learning. By effectively integrating diffusion models with reinforcement learning, DIVER enables the generation of diverse trajectories. Compared with state-of-the-art approaches, our method demonstrates superior performance in both diversity and safety across multiple benchmarks such as Bench2Drive, NAVSIM, and nuScenes, highlighting its potential for robust and flexible autonomous planning in

complex real-world scenarios. While the proposed DIVER emphasizes trajectory diversity, ensuring the correctness of trajectory selection remains a challenge. In future work, we plan to integrate the Vision-Language-Action model to jointly optimize trajectory generation and decision-making for safer planning.

## ACKNOWLEDGMENTS

This work was supported in part by the National Key R&D Program of China (2018AAA0100302), supported by the STI 2030-Major Projects under Grant 2021ZD0201404.

## REFERENCES

- [1] Y. Hu, J. Yang, L. Chen, K. Li, C. Sima, X. Zhu, S. Chai, S. Du, T. Lin, W. Wang, L. Lu, X. Jia, Q. Liu, J. Dai, Y. Qiao, and H. Li, "Planning-oriented autonomous driving," in *Proceedings of the IEEE/CVF Conference on Computer Vision and Pattern Recognition (CVPR)*, June 2023, pp. 17853–17862.
- [2] B. Jiang, S. Chen, Q. Xu, B. Liao, J. Chen, H. Zhou, Q. Zhang, W. Liu, C. Huang, and X. Wang, "Vad: Vectorized scene representation for efficient autonomous driving," in *Proceedings of the IEEE/CVF International Conference on Computer Vision*, 2023, pp. 8340–8350.
- [3] W. Sun, X. Lin, Y. Shi, C. Zhang, H. Wu, and S. Zheng, "Sparsedrive: End-to-end autonomous driving via sparse scene representation," *arXiv preprint arXiv:2405.19620*, 2024.
- [4] B. Liao, S. Chen, H. Yin, B. Jiang, C. Wang, S. Yan, X. Zhang, X. Li, Y. Zhang, Q. Zhang *et al.*, "Diffusiondrive: Truncated diffusion model for end-to-end autonomous driving," *arXiv preprint arXiv:2411.15139*, 2024.
- [5] K. Chitta, A. Prakash, B. Jaeger, Z. Yu, K. Renz, and A. Geiger, "Transfuser: Imitation with transformer-based sensor fusion for autonomous driving," *IEEE Transactions on Pattern Analysis and Machine Intelligence*, vol. 45, no. 11, pp. 12 878–12 895, 2023.
- [6] D. Xu, H. Li, Q. Wang, Z. Song, L. Chen, and H. Deng, "M2da: Multi-modal fusion transformer incorporating driver attention for autonomous driving," *arXiv preprint arXiv:2403.12552*, 2024.
- [7] S. Hu, L. Chen, P. Wu, H. Li, J. Yan, and D. Tao, "St-p3: End-to-end vision-based autonomous driving via spatial-temporal feature learning," in *European Conference on Computer Vision*. Springer, 2022, pp. 533–549.
- [8] S. Chen, B. Jiang, H. Gao, B. Liao, Q. Xu, Q. Zhang, C. Huang, W. Liu, and X. Wang, "Vadv2: End-to-end vectorized autonomous driving via probabilistic planning," *arXiv preprint arXiv:2402.13243*, 2024.
- [9] Z. Li, K. Li, S. Wang, S. Lan, Z. Yu, Y. Ji, Z. Li, Z. Zhu, J. Kautz, Z. Wu *et al.*, "Hydra-mdp: End-to-end multimodal planning with multi-target hydra-distillation," *arXiv preprint arXiv:2406.06978*, 2024.
- [10] L. Chen, P. Wu, K. Chitta, B. Jaeger, A. Geiger, and H. Li, "End-to-end autonomous driving: Challenges and frontiers," *IEEE Transactions on Pattern Analysis and Machine Intelligence*, 2024.
- [11] Z. Song, L. Liu, F. Jia, Y. Luo, C. Jia, G. Zhang, L. Yang, and L. Wang, "Robustness-aware 3d object detection in autonomous driving: A review and outlook," *IEEE Transactions on Intelligent Transportation Systems*, pp. 1–30, 2024.
- [12] Y. Choi, R. C. Mercurius, S. M. A. Shabestary, and A. Rasouli, "Dice: Diverse diffusion model with scoring for trajectory prediction," in *2024 IEEE Intelligent Vehicles Symposium (IV)*. IEEE, 2024, pp. 3023–3029.
- [13] X. Chen, J. Yan, W. Liao, T. He, and P. Peng, "Int2planner: An intention-based multi-modal motion

planner for integrated prediction and planning," *arXiv preprint arXiv:2501.12799*, 2025.

[14] J. Ho, A. Jain, and P. Abbeel, "Denoising diffusion probabilistic models," *Advances in neural information processing systems*, vol. 33, pp. 6840–6851, 2020.

[15] C. Chi, Z. Xu, S. Feng, E. Cousineau, Y. Du, B. Burchfiel, R. Tedrake, and S. Song, "Diffusion policy: Visuomotor policy learning via action diffusion," *The International Journal of Robotics Research*, p. 02783649241273668, 2023.

[16] L. Yang, Z. Zhang, Y. Song, S. Hong, R. Xu, Y. Zhao, W. Zhang, B. Cui, and M.-H. Yang, "Diffusion models: A comprehensive survey of methods and applications," *ACM Computing Surveys*, vol. 56, no. 4, pp. 1–39, 2023.

[17] D. Guo, D. Yang, H. Zhang, J. Song, R. Zhang, R. Xu, Q. Zhu, S. Ma, P. Wang, X. Bi *et al.*, "Deepseek-r1: Incentivizing reasoning capability in llms via reinforcement learning," *arXiv preprint arXiv:2501.12948*, 2025.

[18] B. Jiang, S. Chen, Q. Zhang, W. Liu, and X. Wang, "Alphadrive: Unleashing the power of vlms in autonomous driving via reinforcement learning and reasoning," *arXiv preprint arXiv:2503.07608*, 2025.

[19] H. Gao, S. Chen, B. Jiang, B. Liao, Y. Shi, X. Guo, Y. Pu, H. Yin, X. Li, X. Zhang *et al.*, "Rad: Training an end-to-end driving policy via large-scale 3dgs-based reinforcement learning," *arXiv preprint arXiv:2502.13144*, 2025.

[20] P. Wu, X. Jia, L. Chen, J. Yan, H. Li, and Y. Qiao, "Trajectory-guided control prediction for end-to-end autonomous driving: A simple yet strong baseline," in *Advances in Neural Information Processing Systems*, S. Koyejo, S. Mohamed, A. Agarwal, D. Belgrave, K. Cho, and A. Oh, Eds., vol. 35. Curran Associates, Inc., 2022, pp. 6119–6132. [Online]. Available: [https://proceedings.neurips.cc/paper\\_files/paper/2022/file/286a371d8a0a559281f682f8fbf89834-Paper-Conference.pdf](https://proceedings.neurips.cc/paper_files/paper/2022/file/286a371d8a0a559281f682f8fbf89834-Paper-Conference.pdf)

[21] W. Zeng, W. Luo, S. Suo, A. Sadat, B. Yang, S. Casas, and R. Urtasun, "End-to-end interpretable neural motion planner," in *2019 IEEE/CVF Conference on Computer Vision and Pattern Recognition (CVPR)*, Jun 2019. [Online]. Available: <http://dx.doi.org/10.1109/cvpr.2019.00886>

[22] A. Vaswani, N. Shazeer, N. Parmar, J. Uszkoreit, L. Jones, A. N. Gomez, Ł. Kaiser, and I. Polosukhin, "Attention is all you need," *Advances in neural information processing systems*, vol. 30, 2017.

[23] Z. Song, L. Yang, S. Xu, L. Liu, D. Xu, C. Jia, F. Jia, and L. Wang, "Graphbev: Towards robust bev feature alignment for multi-modal 3d object detection," *arXiv preprint arXiv:2403.11848*, 2024.

[24] Z. Song, H. Wei, L. Bai, L. Yang, and C. Jia, "Graphalign: Enhancing accurate feature alignment by graph matching for multi-modal 3d object detection," in *Proceedings of the IEEE/CVF International Conference on Computer Vision*, 2023, pp. 3358–3369.

[25] Z. Li, W. Wang, H. Li, E. Xie, C. Sima, T. Lu, Y. Qiao, and J. Dai, "Bevformer: Learning bird's-eye-view representation from multi-camera images via spatiotemporal transformers," in *European conference on computer vision*. Springer, 2022, pp. 1–18.

[26] T. Meinhardt, A. Kirillov, L. Leal-Taixé, and C. Feichtenhofer, "Trackformer: Multi-object tracking with transformers," *Cornell University - arXiv*, Cornell University - arXiv, Jan 2021.

[27] B. Liao, S. Chen, X. Wang, T. Cheng, Q. Zhang, W. Liu, and C. Huang, "Maptr: Structured modeling and learning for online vectorized hd map construction," *arXiv preprint arXiv:2208.14437*, 2022.

[28] S. Shi, L. Jiang, D. Dai, and B. Schiele, "Mtr++: Multi-agent motion prediction with symmetric scene modeling and guided intention querying," *IEEE Transactions on Pattern Analysis and Machine Intelligence*, 2024.

[29] P. Tang, Z. Wang, G. Wang, J. Zheng, X. Ren, B. Feng, and C. Ma, "Sparseocc: Rethinking sparse latent representation for vision-based semantic occupancy prediction," in *Proceedings of the IEEE/CVF Conference on Computer Vision and Pattern Recognition*, 2024, pp. 15 035–15 044.

[30] P. Cai and D. Hsu, "Closing the planning–learning loop with application to autonomous driving," *IEEE Transactions on Robotics*, vol. 39, no. 2, pp. 998–1011, 2022.

[31] S. Doll, N. Hanselmann, L. Schneider, R. Schulz, M. Cordts, M. Enzweiler, and H. Lensch, "Dualad: Disentangling the dynamic and static world for end-to-end driving," in *Proceedings of the IEEE/CVF Conference on Computer Vision and Pattern Recognition*, 2024, pp. 14 728–14 737.

[32] Z. Chen, M. Ye, S. Xu, T. Cao, and Q. Chen, "Ppad: Iterative interactions of prediction and planning for end-to-end autonomous driving," in *European Conference on Computer Vision*. Springer, 2025, pp. 239–256.

[33] Z. Song, C. Jia, L. Liu, H. Pan, Y. Zhang, J. Wang, X. Zhang, S. Xu, L. Yang, and Y. Luo, "Don't shake the wheel: Momentum-aware planning in end-to-end autonomous driving," 2025. [Online]. Available: <https://arxiv.org/abs/2503.03125>

[34] X. Wang, Z. Zhu, G. Huang, X. Chen, J. Zhu, and J. Lu, "Drivedreamer: Towards real-world-drive world models for autonomous driving," in *European Conference on Computer Vision*. Springer, 2024, pp. 55–72.

[35] C. Xu, A. Petrushko, D. Zhao, and B. Li, "Diffscene: Diffusion-based safety-critical scenario generation for autonomous vehicles," in *Proceedings of the AAAI Conference on Artificial Intelligence*, vol. 39, no. 8, 2025, pp. 8797–8805.

[36] J. Zou, K. Tian, Z. Zhu, Y. Ye, and X. Wang, "Diffbev: Conditional diffusion model for bird's eye view perception," in *Proceedings of the AAAI conference on artificial intelligence*, vol. 38, no. 7, 2024, pp. 7846–7854.

[37] C. Jiang, A. Cornman, C. Park, B. Sapp, Y. Zhou, D. Anguelov *et al.*, "Motiondiffuser: Controllable multi-agent motion prediction using diffusion," in *Proceedings of the IEEE/CVF conference on computer vision and pattern recognition*, 2023, pp. 9644–9653.

[38] Z. Guo, K. Gubernatorov, S. Asfaw, Z. Yagudin, and D. Tsetserukou, "Vdt-auto: End-to-end autonomous driving with vlm-guided diffusion transformers," *arXiv preprint arXiv:2502.20108*, 2025.

[39] T. Wang, C. Zhang, X. Qu, K. Li, W. Liu, and C. Huang, "Diffad: A unified diffusion modeling approach for autonomous driving," *arXiv preprint arXiv:2503.12170*, 2025.

[40] H. Su, W. Wu, and J. Yan, "Difsd: Ego-centric fully sparse paradigm with uncertainty denoising and iterative refinement for efficient end-to-end autonomous driving," *arXiv preprint arXiv:2409.09777*, 2024.

[41] X. Wang, S. Wang, X. Liang, D. Zhao, J. Huang, X. Xu, B. Dai, and Q. Miao, "Deep reinforcement learning: A survey," *IEEE Transactions on Neural Networks and Learning Systems*, vol. 35, no. 4, pp. 5064–5078, 2022.

[42] D. Silver, A. Huang, C. J. Maddison, A. Guez, L. Sifre, G. Van Den Driessche, J. Schrittwieser, I. Antonoglou, V. Panneershelvam, M. Lanctot *et al.*, "Mastering the game of go with deep neural networks and tree search," *nature*, vol. 529, no. 7587, pp. 484–489, 2016.

[43] D. Silver, J. Schrittwieser, K. Simonyan, I. Antonoglou, A. Huang, A. Guez, T. Hubert, L. Baker, M. Lai, A. Bolton *et al.*, "Mastering the game of go without human knowledge," *nature*, vol. 550, no. 7676, pp. 354–359, 2017.

[44] J. Jumper, R. Evans, A. Pritzel, T. Green, M. Figurnov, O. Ronneberger, K. Tunyasuvunakool, R. Bates, A. Žídek, A. Potapenko *et al.*, "Highly accurate protein structure prediction with alphafold," *nature*, vol. 596, no. 7873, pp. 583–589, 2021.

[45] D. Chen, V. Koltun, and P. Krähenbühl, "Learning to drive from a world on rails," in *Proceedings of the IEEE/CVF International Conference on Computer Vision*, 2021, pp. 15 590–

15 599.

[46] Y. Hu, S. Chai, Z. Yang, J. Qian, K. Li, W. Shao, H. Zhang, W. Xu, and Q. Liu, "Solving motion planning tasks with a scalable generative model," in *European Conference on Computer Vision*. Springer, 2024, pp. 386–404.

[47] Y. Lu, J. Fu, G. Tucker, X. Pan, E. Bronstein, R. Roelofs, B. Sapp, B. White, A. Faust, S. Whiteson *et al.*, "Imitation is not enough: Robustifying imitation with reinforcement learning for challenging driving scenarios," in *2023 IEEE/RSJ International Conference on Intelligent Robots and Systems (IROS)*. IEEE, 2023, pp. 7553–7560.

[48] M. Toromanoff, E. Wirbel, and F. Moutarde, "End-to-end model-free reinforcement learning for urban driving using implicit affordances," in *Proceedings of the IEEE/CVF conference on computer vision and pattern recognition*, 2020, pp. 7153–7162.

[49] Z. Zhang, A. Liniger, D. Dai, F. Yu, and L. Van Gool, "End-to-end urban driving by imitating a reinforcement learning coach," in *Proceedings of the IEEE/CVF international conference on computer vision*, 2021, pp. 15 222–15 232.

[50] X. Jia, Z. Yang, Q. Li, Z. Zhang, and J. Yan, "Bench2drive: Towards multi-ability benchmarking of closed-loop end-to-end autonomous driving," *arXiv preprint arXiv:2406.03877*, 2024.

[51] H. Caesar, V. Bankiti, A. H. Lang, S. Vora, V. E. Liong, Q. Xu, A. Krishnan, Y. Pan, G. Baldan, and O. Beijbom, "nuscenes: A multimodal dataset for autonomous driving," in *Proceedings of the IEEE/CVF conference on computer vision and pattern recognition*, 2020, pp. 11 621–11 631.

[52] J. Schulman, F. Wolski, P. Dhariwal, A. Radford, and O. Klimov, "Proximal policy optimization algorithms," *arXiv preprint arXiv:1707.06347*, 2017.

[53] Z. Shao, P. Wang, Q. Zhu, R. Xu, J. Song, X. Bi, H. Zhang, M. Zhang, Y. Li, Y. Wu *et al.*, "Deepseekmath: Pushing the limits of mathematical reasoning in open language models," *arXiv preprint arXiv:2402.03300*, 2024.

[54] A. Dosovitskiy, G. Ros, F. Codevilla, A. Lopez, and V. Koltun, "CARLA: An open urban driving simulator," in *Proceedings of the 1st Annual Conference on Robot Learning*, ser. Proceedings of Machine Learning Research, S. Levine, V. Vanhoucke, and K. Goldberg, Eds., vol. 78. PMLR, 13–15 Nov 2017, pp. 1–16. [Online]. Available: <https://proceedings.mlr.press/v78/dosovitskiy17a.html>

[55] D. Dauner, M. Hallgarten, T. Li, X. Weng, Z. Huang, Z. Yang, H. Li, I. Gilitschenski, B. Ivanovic, M. Pavone *et al.*, "Navsim: Data-driven non-reactive autonomous vehicle simulation and benchmarking," *Advances in Neural Information Processing Systems*, vol. 37, pp. 28 706–28 719, 2024.

[56] O. Contributors, "Openscene: The largest up-to-date 3d occupancy prediction benchmark in autonomous driving," 2023.

[57] H. Caesar, J. Kabzan, K. S. Tan, W. K. Fong, E. Wolff, A. Lang, L. Fletcher, O. Beijbom, and S. Omari, "nuplan: A closed-loop ml-based planning benchmark for autonomous vehicles," *arXiv preprint arXiv:2106.11810*, 2021.

[58] Z. Song, C. Jia, L. Liu, H. Pan, Y. Zhang, J. Wang, X. Zhang, S. Xu, L. Yang, and Y. Luo, "Don't shake the wheel: Momentum-aware planning in end-to-end autonomous driving," 2025.

[59] Z. Xu, B. Li, H.-a. Gao, M. Gao, Y. Chen, M. Liu, C. Yan, H. Zhao, S. Feng, and H. Zhao, "Challenger: Affordable adversarial driving video generation," *arXiv preprint arXiv:2505.15880*, 2025.

[60] Y. Dong, C. Kang, J. Zhang, Z. Zhu, Y. Wang, X. Yang, H. Su, X. Wei, and J. Zhu, "Benchmarking robustness of 3d object detection to common corruptions," in *Proceedings of the IEEE/CVF Conference on Computer Vision and Pattern Recognition (CVPR)*, June 2023, pp. 1022–1032.

[61] X. Jia, P. Wu, L. Chen, J. Xie, C. He, J. Yan, and H. Li, "Think twice before driving: Towards scalable decoders for end-to-end autonomous driving," in *Proceedings of the IEEE/CVF Conference on Computer Vision and Pattern Recognition (CVPR)*, June 2023, pp. 21 983–21 994.

[62] X. Jia, Y. Gao, L. Chen, J. Yan, P. L. Liu, and H. Li, "Driveadapter: Breaking the coupling barrier of perception and planning in end-to-end autonomous driving," in *Proceedings of the IEEE/CVF International Conference on Computer Vision*, 2023, pp. 7953–7963.

[63] X. Jia, J. You, Z. Zhang, and J. Yan, "Drivetransformer: Unified transformer for scalable end-to-end autonomous driving," *arXiv preprint arXiv:2503.07656*, 2025.

[64] Y. Li, Y. Wang, Y. Liu, J. He, L. Fan, and Z. Zhang, "End-to-end driving with online trajectory evaluation via bev world model," *arXiv preprint arXiv:2504.01941*, 2025.

[65] J.-T. Zhai, Z. Feng, J. Du, Y. Mao, J.-J. Liu, Z. Tan, Y. Zhang, X. Ye, and J. Wang, "Rethinking the open-loop evaluation of end-to-end autonomous driving in nuscenes," *arXiv preprint arXiv:2305.10430*, 2023.

[66] W. Zheng, R. Song, X. Guo, and L. Chen, "Genad: Generative end-to-end autonomous driving," *arXiv preprint arXiv:2402.11502*, 2024.

[67] X. Weng, B. Ivanovic, Y. Wang, Y. Wang, and M. Pavone, "Para-drive: Parallelized architecture for real-time autonomous driving," in *Proceedings of the IEEE/CVF Conference on Computer Vision and Pattern Recognition*, 2024, pp. 15 449–15 458.

[68] K. He, X. Zhang, S. Ren, and J. Sun, "Deep residual learning for image recognition," in *Proceedings of the IEEE conference on computer vision and pattern recognition*, 2016, pp. 770–778.

**Ziying Song** was born in Xingtai, Hebei Province, China in 1997. He received the B.S. degree from Hebei Normal University of Science and Technology (China) in 2019. He received a master's degree major in Hebei University of Science and Technology (China) in 2022. He is now a PhD student majoring in Computer Science and Technology at Beijing Jiaotong University (China), with a research focus on Computer Vision.



**Lin Liu** was born in Jinzhou, Liaoning Province, China, in 2001. He is now a college student majoring in Computer Science and Technology at China University of Geosciences (Beijing). Since Dec. 2022, he has been recommended for a master's degree in Computer Science and Technology at Beijing Jiaotong University. His research interests are in computer vision.





**Hongyu Pan** received the B.E. degree from Beijing Institute of Technology (BIT) in 2016 and the M.S. degree in computer science from the Institute of Computing Technology (ICT), University of Chinese Academy of Sciences (UCAS), in 2019. He is currently an employee at Horizon Robotics. His research interests include computer vision, pattern recognition, and image processing. He specifically focuses on 3D detection/segmentation/motion and depth estimation.



Robotics.

**Shaoqing Xu** received his M.S. degree in transportation engineering from the School of Transportation Science and Engineering in Beihang University. He is currently working toward the Ph.D. degree in electromechanical engineering with the State Key Laboratory of Internet of Things for Smart City, University of Macau, Macao SAR, China. His research interests include 3D Space Intelligence, End2End, WorldModel, Vision-Language-Action(VLA), and its applications in Autonomous Driving and



**Bencheng Liao** received the B.E. degree from School of Electronic Information and Communications, Huazhong University of Science and Technology, Wuhan, China, in 2020. He is currently a PhD candidate at the Institute of Artificial Intelligence and School of Electronic Information and Communications, Huazhong University of Science and Technology. His research interests include object detection, 3D vision, and autonomous driving.



**Mingzhe Guo** is a Ph.D. candidate working on computer vision and deep learning at Beijing Key Lab of Traffic Data Analysis and Mining, Beijing Jiaotong University as of 2020. Before that he received the B.S. degree at Beijing Jiaotong University in 2020. He is about to work as a researcher at Baidu Inc. His research interest includes visual object tracking, BEV detection/tracking and E2E-AD.



**Caiyan Jia**, born on March 2, 1976, is a lecturer and a postdoctoral fellow of the Chinese Computer Society. She graduated from Ningxia University in 1998 with a bachelor's degree in mathematics, Xiangtan University in 2001 with a master's degree in computational mathematics, specializing in intelligent information processing, and the Institute of Computing Technology of the Chinese Academy of Sciences in 2004 with a doctorate degree in engineering, specializing in data mining. She has received her D. degree in 2004. She is now a professor in School of Computer Science and Technology, Beijing Jiaotong University, Beijing, China.



3D scene understanding and world model.

**Lei Yang (Member, IEEE)** received his M.S. degree from the Robotics Institute at Beihang University, in 2018, and the Ph.D. degree from the School of Vehicle and Mobility, Tsinghua University, in 2024. From 2018 to 2020, he joined the Autonomous Driving R&D Department of JD.COM as an algorithm researcher. Currently, he is a research fellow with the School of Mechanical and Aerospace Engineering, Nanyang Technological University, Singapore. His current research interests include autonomous driving, 3D scene understanding and world model.



**Yadan Luo (Member, IEEE)** received the BS degree in computer science from the University of Electronic Science and Technology of China, and the PhD degree from the University of Queensland. Her research interests include machine learning, computer vision, and multimedia data analysis. She is now a lecturer with the University of Queensland.



**Yongchang Zhang** received the B.E. degree from the University of Electronic Science and Technology of China (UESTC) in 2020 and the M.S. degree in control theory and control engineering from the Institute of Automation (CASIA), University of Chinese Academy of Sciences (UCAS) in 2023. He is currently a Research Engineer at Horizon Robotics. His research interests include computer vision, autonomous driving perception, and visual-language models.